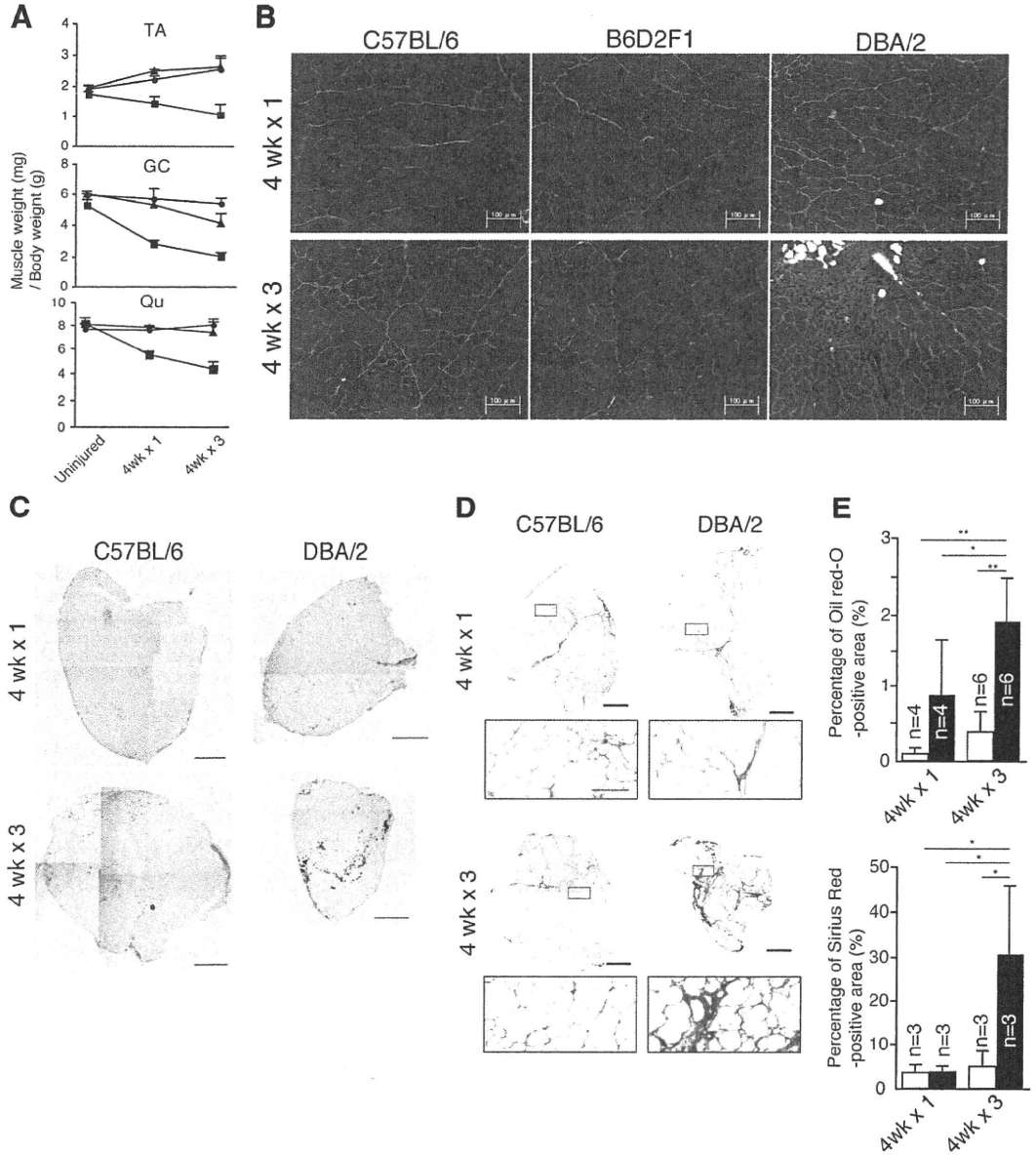

Figure 2. Impaired regeneration of DBA/2 phenotype is recessively inherited. **A:** The TA, GC, and Qu muscle weights (mg) per body weight (g) in C57BL/6 (closed circles), DBA/2 (closed squares), and B6D2F1 (closed triangles) mice after one (4 weeks × 1) or three CTX injections (4 weeks × 3). The cross sections were stained with H&E (**B**), Oil red-O (**C**), or Sirius Red (**D**). Scale bars: 100 μm (**B**); 500 μm (**C** and **D**). **E:** The *y* axis shows the mean percentage of Oil red-O or Sirius Red-positive areas per section. White and black columns indicate the results of C57BL/6 and DBA/2, respectively. The number in the each graph indicates the number of mice used in this analysis. $^{*}P < 0.05$, $^{**}P < 0.01$ (analysis of variance, SNK-test).

2-*mdx* (D2-*mdx*) mice showed the decreased body weight regardless of gender (Figure 5A). A more remarkable phenotype of D2-*mdx* was the loss of skeletal muscle mass (Figure 5B). As previously reported, the muscle weight of B10-*mdx* was heavier than that of controls,[8] but the TA, GC, and Qu muscle weights of D2-*mdx* males were 71%, 59%, and 54% of those of controls, respectively (Figure 5C). Female muscles were 85% (TA), 61% (GC), and 52% (Qu) of each control muscle, respectively. The loss of muscle weight did not simply reflect the decreased body weight because there is also a significant difference in muscle weight (mg) per body weight (g) between D2-*mdx* and control littermates (Figure 5C). Control littermates of D2-*mdx* and normal DBA/2 exhibited similar results in muscle weight per body weight ratios (data not shown).

Histology of DBA/2-mdx

In contrast to the histology of DMD, it is widely accepted that fibrosis and fat replacement are minimal in B10-*mdx*.[7] In addition, there was no apparent fiber loss. To examine the accumulation of fibrosis and fat tissue in D2-*mdx*, cross sections were stained with Sirius Red or Oil red-O. As shown in Figure 6, A and B, there was no sign of fibrosis or adipogenesis in B10-*mdx*. However, D2-*mdx* mice exhibited increased fibrosis and fat accu-

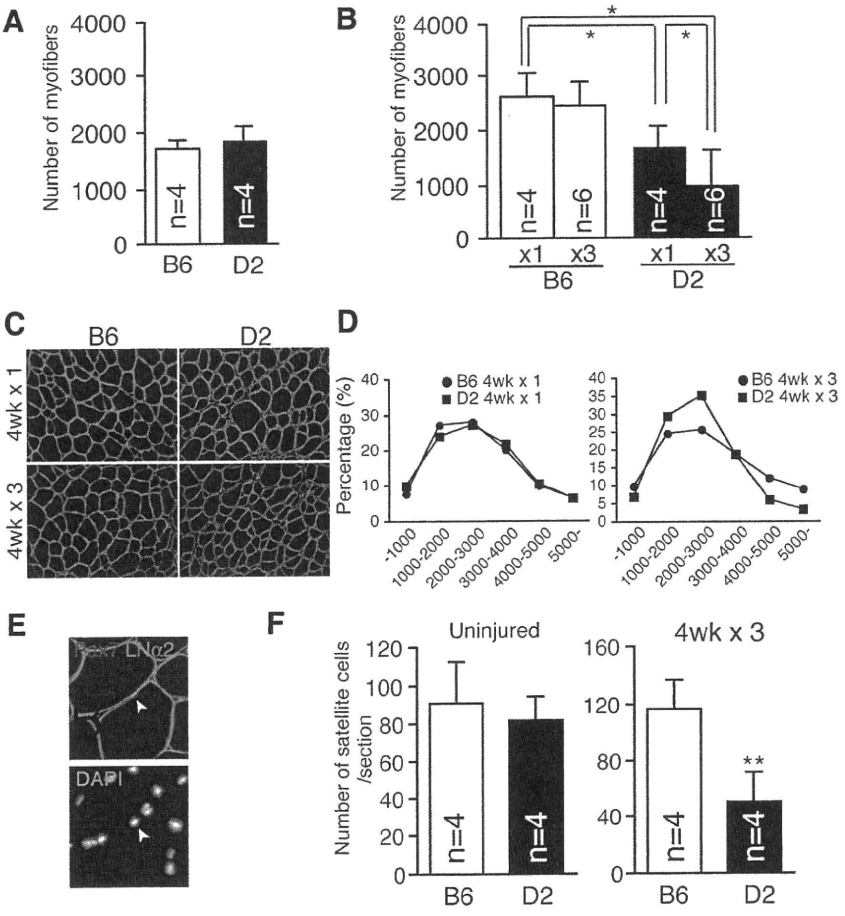

Figure 3. Decreased numbers of myofibers and satellite cells in DBA/2 mice after three repeated injuries. **A:** The number of myofibers in uninjured TA muscle at 10 weeks old. The *y* axis shows the mean number of myofibers per section. B6 and D2 indicate C57BL/6 and DBA/2, respectively. **B:** The mean numbers of myofiber in TA muscles after one or three injuries. $^{*}P < 0.05$ (analysis of variance, SNK-test). The sizes of myofibers in TA muscle after one or three CTX injections. **C:** Cross sections were stained with anti-laminin α2 antibody (green). **D:** The size of each myofiber in TA muscle was measured after one or three injections. Closed circles or squares show the results of C57BL/6 or DBA/2, respectively. **E: Arrowhead** indicates Pax7 expressing cells lying beneath the basal lamina. **F:** The number of satellite cells in noninjured TA muscle (uninjured) or TA muscle injured three times (4 weeks × 3). The *y* axis shows the mean number of satellite cells per section. The number in each graph indicates the number of mice used in these analyses. $^{**}P < 0.01$ (Student's *t*-test).

mulation in comparison with B10-*mdx*. In contrast to B10-*mdx*, a decreased number of total myofibers was also observed in D2-*mdx* (Figure 6C).

To enumerate the number of necrotic fibers, the mice were injected with Evans blue dye to visualize necrotic fibers. As shown in Figure 6C, fewer total necrotic fibers were observed in D2-*mdx*. This result suggests that the D2-*mdx* phenotype does not result from acceleration of degeneration.

Decreased Skeletal Muscle Function in DBA/2-mdx

Skeletal muscle endurance was assessed by treadmill running to exhaustion as an indicator of maximal muscle capacity. After acclimatization, mice were run on a 10% slope at increasing speed until the animals were unable to remain on the treadmill despite prodding. We then recorded the end time and speed to calculate the distance run. As shown in Figure 7A, male and female D2-*mdx* ran 45% and 56% shorter distances than control littermates. The maximum speed of D2-*mdx* was also lower than that of their littermate. The distance run showed the most significantly difference because of the protocol of increasing speed (Figure 7A). The average distance run by male controls was 544 meters, but that of D2-*mdx* males was 205 meters (38% of the control). A similar result was shown by female D2-*mdx* (25% of the control). B10-*mdx* also showed lower values compared with normal C57BL/10 mice (data not shown), but the decreased ratio of each parameter in D2-*mdx* was more remarkable than that in B10-*mdx* (Figure 7B).

A grip strength test was also performed as an indicator of motor function and whether D2-*mdx* exhibited muscle weakness compared with controls. As shown in Figure 7C, D2-*mdx* earned a lower score than control mice regardless of gender. However, there was no significant difference between B10-*mdx* and control mice.

Discussion

Repeated Injury Models

Muscle satellite cells play central roles in skeletal muscle regeneration.[23] Satellite cells produce a vast number of progenitor cells (myoblasts) that finally become myofibers. During this process, at least some of the satellite cells have self-renewal potential,[14,24] but are quiescent and will respond efficiently to the next damages. In fact, Luz et al[15] indicated that C57BL/10 could regenerate after 50 bupivacaine injections without the loss of myofibers or gain of fibrotic areas in the TA muscle. Importantly, C57BL/10-*mdx* mice exhibited decreased numbers of myofibers after 50 bupivacaine injections[15]

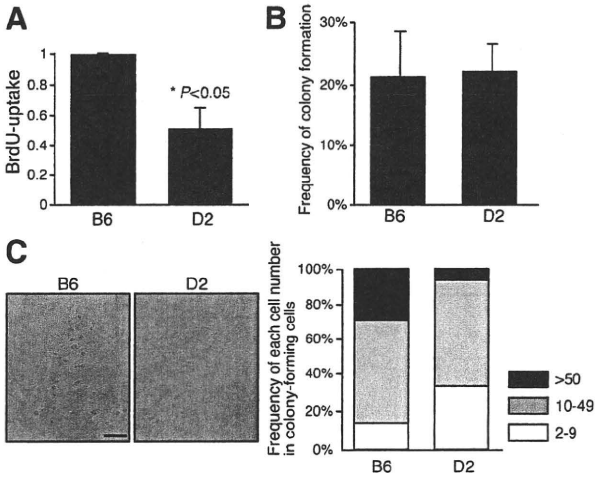

Figure 4. Satellite cells of DBA/2 strain show inferior BrdU uptake and colony-forming potential. **A:** BrdU uptake of primary myoblasts derived from C57BL/6 or DBA/2 satellite cells. The *y* axis shows the mean with SD of three independent experiments. $*P < 0.05$ (Student's *t*-test). Frequency of colony formation by a single satellite cell derived from C57BL/6 or DBA/2 (**B**) and the size of single cell-derived colonies (**C**). The picture shows representative colonies of each strain. Colonies were categorized into three groups: >50 cells/well, 10 to 49 cells/well, and 2 to 9 cells/well. The *y* axis indicates the frequency (**B**) or percentage of each category (**C**) from three independent experiments. Scale bar = 100 μm.

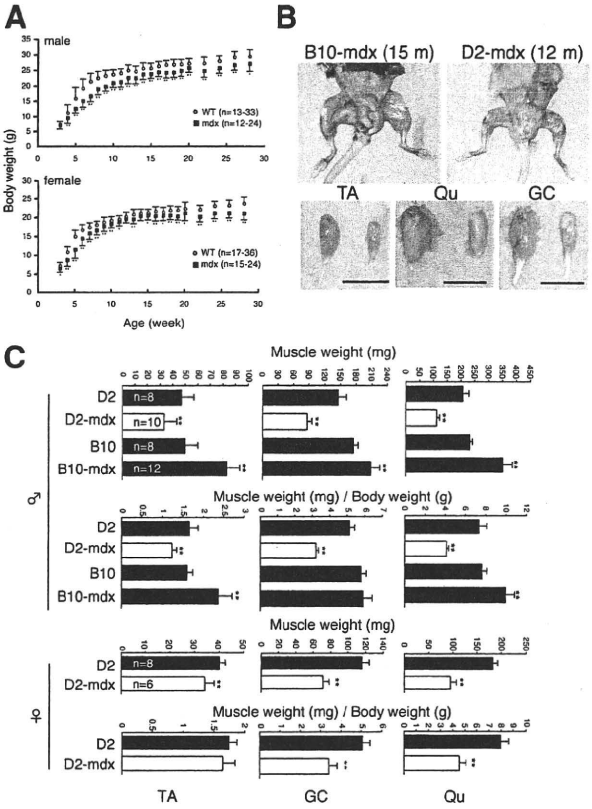

Figure 5. DBA/2-*mdx* mice show decreased body weight and remarkable muscle weight loss. **A:** Body weight of D2-*mdx* (closed squares) and their wild or heterozygous littermates (open circles) related to age. $*P < 0.05$, $**P < 0.01$ (Student's *t*-test) **B:** Photographs of hind limb muscles of male B10-*mdx* (15 months) and D2-*mdx* (12 months). Scale bar = 1 cm. **C:** TA, GC, and Qu muscle weights (mg) or per body weight (g) of 6-month-old mice. *x* axis shows the mean with SD. The numbers of muscles used in each study are shown in each graph. $*P < 0.05$, $**P < 0.01$.

because C57BL10-*mdx* mice already have dystrophic degeneration–regeneration cycles. Sadeh et al[25] also showed active regeneration cycles in rats that received weekly injections of bupivacaine for 6 months. They reported that there was lack of evidence for reduction or exhaustion of muscle fiber capacity to regenerate despite ongoing degeneration–regeneration over a period approximating one fourth of the rat life expectancy. These results indicate that the satellite cell pool was efficiently maintained for multiple degeneration–regeneration cycles in these animals, and that dystrophic mice exhibit less regeneration ability. However, DBA/2 showed significantly decreased numbers of myofibers and self-renewed satellite cells after only three injections of CTX.

The number of DBA/2 satellite cells in uninjured TA muscle is similar to that of C57BL/6. Although, the myofibers in DBA/2 were smaller than those in C57BL/6 2 weeks after one CTX injection (data not shown), the myofiber size and histological characteristics showed few significant differences between and DBA/2 and C57BL/6 4 weeks after a single CTX injection. These results suggest that the self-renewal ability of DBA/2 satellite cells is incomplete and that the exhaustion of muscle satellite cells leads to a decreased number of myofiber and loss of skeletal muscle weight. Nonmyogenic cells, for example, macrophages, also play important roles in skeletal muscle regeneration. However, dysfunction of macrophages leads to impaired regeneration after one CTX injection.[26,27] Furthermore, the remarkable regeneration deficit was not observed in DBA/2 4 weeks after one CTX injection in TA muscle. These results suggest that repeated injury is a suitable model to assess the long-term regeneration potential of skeletal muscle, and that the self-renewal ability of satellite cells is responsible at least in part for the result of repeatedly injured muscle in DBA/2.

Strain Differences of Muscle Regeneration Ability

C57BL/6, a strain akin to C57BL/10, is the most widely used strain for skeletal muscle regeneration studies. As shown in Figure 1, C57BL/6 has the best ability to regenerate skeletal muscle among the four inbred strains examined. An early study by Grounds and McGeachie[28] indicated a strain difference in skeletal muscle regeneration between BALB/c and Swiss SJL/J. They showed that superior and faster regeneration was observed in the Swiss SJL/J strain. The most outstanding phenotype of DBA/2 is the remarkable decrease of muscle weight compared with the three other inbred strains, including BALB/c. Intriguingly, DBA/2 mice have a shorter life span than C57BL/6.[29] In addition, it is reported that muscle weight loss is increased during aging (sarcopenia) in DBA/2 mice compared with C57BL/6.[30] The reason why the DBA/2 strain exhibits the loss of muscle weight is unknown, but our results imply a relationship between

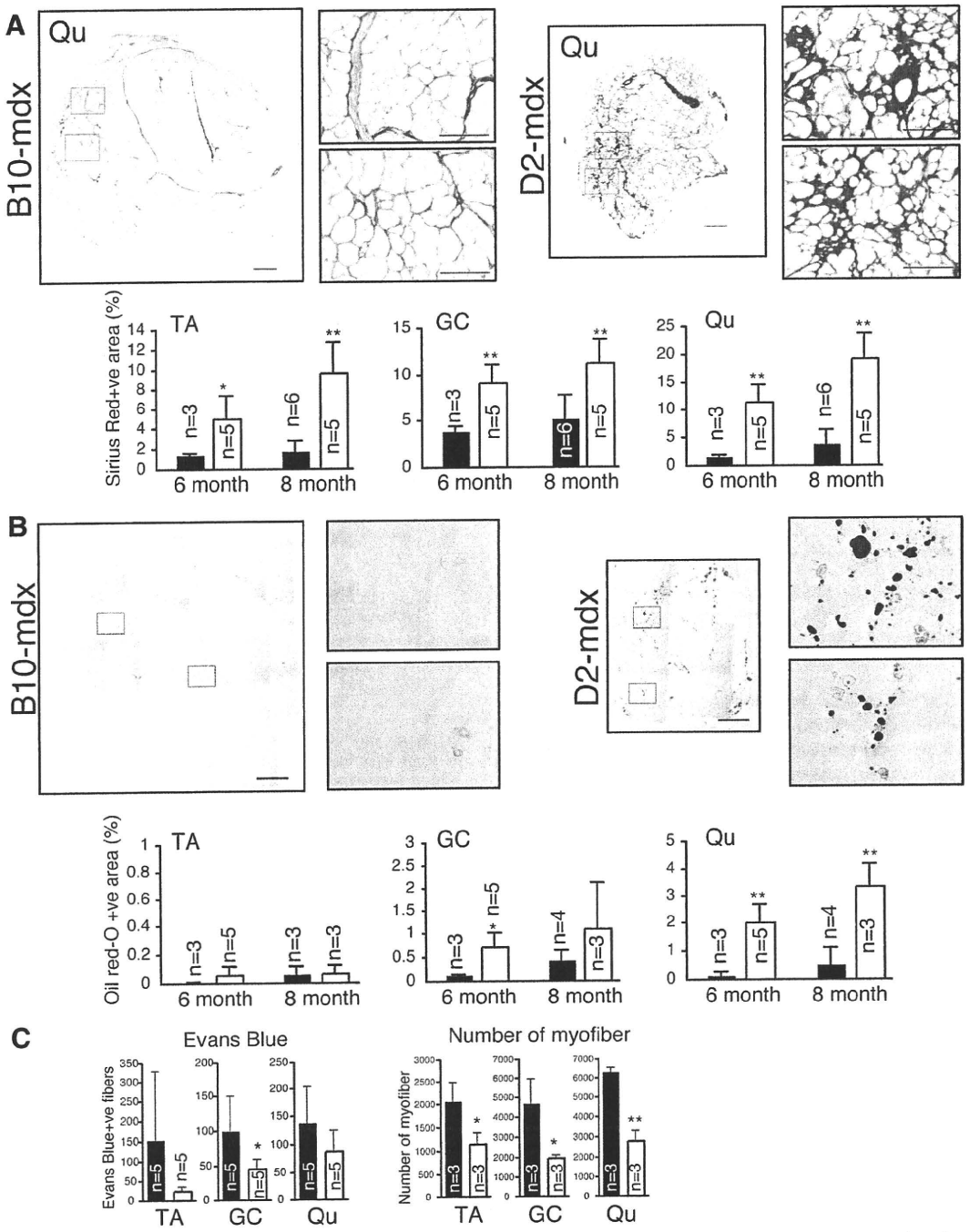

Figure 6. Histological analyses of DBA/2-*mdx* mice. Sirius red staining (**A**) and Oil red-O staining (**B**) of Qu muscle of 8-month-old B10-*mdx* and D2-*mdx* mice. The *y* axis indicates the mean percentage of Sirius Red- (**A**) or Oil red-O (**B**) -positive areas per section. The *x* axis indicates the age of mice. Black and white columns show the results for B10-*mdx* and D2-*mdx*, respectively. The numbers of mice used in each study are shown in each graph. **C:** The *y* axis indicates the mean number of Evans blue-positive or total myofibers of B10-*mdx* and D2-*mdx* at 8 months of age. $^{*}P < 0.05$, $^{**}P < 0.01$.

the impaired function of satellite cells and sarcopenia in DBA/2.

Heydemann et al[31] reported that γ-sarcoglycan-null mice with DBA/2 background showed decreased skeletal muscle weight, increased Evans Blue uptake, and a higher hydroxyproline concentration than C57BL/6, CD1, and 129 background null mice. Although they ruled out the voluntary activities of DBA/2, they did not discuss the cause of these results. Our results suggest that the low regeneration potential of DBA/2 leads to a severe skeletal muscle phenotype in various dystrophic mouse models.

The DBA/2J strain has been used in sarcopenia and γ-sarcoglycan-null mouse studies.[30,31] To exclude the possibility that DBA/2 substrain differences exist, we compared the BrdU uptake of primary myoblasts in DBA/2N (used in this study) and DBA/2J. Because we observed similar low BrdU uptakes by primary myoblasts in both DBA/2N and DBA/2J (data not shown), these

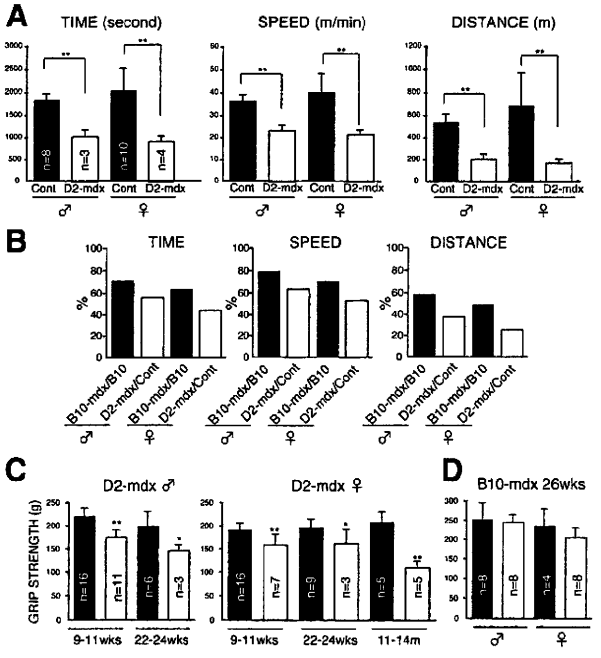

Figure 7. Comparison of muscle strength in DBA/2-*mdx* and B10-*mdx*. **A:** Treadmill running test of mice at 24 weeks old. Final time, speed, and distance were recorded and calculated for the individual performance score. The averages are shown with SD. Control indicates heterozygous or wild-type littermates of D2-*mdx*. The numbers of mice used in each study are shown in each graph. $^{*}P < 0.05$, $^{**}P < 0.01$. **B:** Comparison of C57BL/10-*mdx* and DBA/2-*mdx* in treadmill running test. The *y* axis indicates the percentage of *mdx* per control value. The numbers of male C57BL/10, male C57BL/10-*mdx*, female C57BL/10, and female C57BL/10-*mdx* are 4, 4, 4, and 8, respectively. Grip strength test of D2-*mdx* (**C**) or B10-*mdx* (**D**). Black and white columns indicate the results for *mdx* or control mice, respectively. The *y* axis indicates the average score of each mouse with SD. The *x* axis shows the ages of mice. The number in the each graph indicates the number of mice taking this test. $^{*}P < 0.05$, $^{**}P < 0.01$.

results suggest that lower muscle regeneration is common to the DBA/2 strain.

Stem (Satellite) Cell Function and Mouse Strains

As mentioned above, some previous reports indicated different responses in skeletal muscle regeneration among inbred strains of mice. However, to our knowledge, this is the first evidence that there is an intrinsic difference in satellite cells among inbred mice. The exact relationship between *in vitro* and *in vivo* results of satellite cells is not clear. However, low or slow proliferation of satellite cells might explain the decreased muscle weight and slow regeneration after a single injury in DBA/2 in comparison with C57BL/6 and B6D2F1, which showed increased muscle weight in their TA muscle (Figure 2A). It is unlikely that telomere erosion contributes to the *in vitro* and *in vivo* results of DBA/2 satellite cells because DBA/2 mice have longer telomeres than C57BL/6 mice.[32]

Recently Kuang et al[33] reported that satellite cells are a heterogeneous population of stem cells (satellite stem cells) and committed progenitor cells, and that they can be distinguished from others by Myf5 expression. They showed that Myf5-negative (satellite stem) cells self-renewed three times more frequently than Myf-5-positive (progenitor) cells *in vivo*. Schultz and Lipton[34] first described the heterogeneity of satellite cells by the different colony sizes of each satellite cell and found decreased colony sizes in aging muscle in the rat. Although it was not determined whether satellite stem cells form a large-colonies or not *in vitro*, our results showed that mice having low self-renewing satellite cells (DBA/2) exhibit smaller colony formations than mice having high self-renewing satellite cells (C57BL/6). These results suggest that satellite stem cells may form larger colonies *in vitro*.

In contrast to satellite cells, a highly strain-dependent function of hematopoietic stem cells was reported.[35] Chen et al[36] reported that DBA/2 showed a decline in primitive hematopoietic stem cell function with age, but that it increased with age in C57BL/6 in a *vivo* transplantation study. Recombinant inbred mice, named BXD strains, are available. Using BXD, Liang et al[37] identified latexin as affecting the size of the hematopoietic stem cell population in mice. A similar approach might lead to the discovery of key genes that affect the properties of satellite cells.

DBA/2-mdx *as Model for DMD*

Mdx was discovered a quarter of a century ago.[5] In 1989, the *mdx* mutation, a C to T transition within exon 23, was identified in the dystrophin gene on the X chromosome.[38] Nearly all *mdx* colonies are maintained as homozygous inbred lines; in addition, the difficulty of point mutation typing might impede the effect of genetic background on *mdx* phenotype. However, Amalfitano and Chamberlain[16] reported a rapid and simple typing strategy, and we established DBA/2-*mdx* following their protocol. C57BL/10-*mdx* mice have played central roles in a vast array of pathological, clinical, and physiological studies as a model for DMD. However, they do not reflect human pathology in some aspects, including little fat and fibrosis accumulation, no loss of myofiber numbers, and muscle weight. Recently, Gargioli et al[39] showed that the advanced stage of dystrophy including sclerosis precluded treatment by stem cell therapy. Therefore, assessment of therapeutic effect in more severe disease conditions is needed.

In marked contrast to the severe phenotype observed in DMD, early studies using C57BL/10-*mdx* concluded that they do not show obvious functional disability.[5,7] However, some later reports indicated functional differences between C57BL/10-*mdx* and control mice.[40–43] As shown in Figure 7, C57BL/6-*mdx* also showed muscle weakness in the treadmill test. However, the muscle weakness of DBA/2-*mdx* is more remarkable than that of C57BL/10-*mdx*. Therefore, DBA/2-*mdx* is a more appropriate model to assess skeletal muscle function after therapeutic treatment.

Chamberlain et al[44] reported that the average life spans of female and male C57BL/10-*mdx* mice were 22.5 and 21.5 months, respectively. Pastoret et al[8] also reported that C57BL/10-*mdx* mice have short life spans and that C57BL/10-*mdx* older than 78 weeks exhibit progressive weakness. We have not determined the life span of DBA/2-*mdx*, but it will be clarified in the future. Intrigu-

ingly, Chamberlain et al[44] observed the appearance of rhabdomyosarcoma-like tumors in C57BL/10-*mdx*. They speculate that the lifelong continuous myofiber degeneration and regeneration that characterize this animal model are associated with continuous and massive activation and proliferation of satellite cells, which greatly increase the chance of developing random and spontaneous mutations. To date, we have observed tumors in C57BL/10-*mdx* but not in DBA/2-*mdx*. This observation supports their speculations.

The reasons why *mdx* mice do not show the human-like pathology have been investigated. One reason for the difference between DMD and *mdx* is explained by the presence of utrophin, a homolog of dystrophin. Utrophin is located in the neuromuscular junction in normal muscle. In dystrophic muscle, utrophin is up-regulated in the sarcolemma and compensates for dystrophin function. As shown in Figure 6, the results of Evans blue uptake in DBA/2-*mdx* indicated that the degeneration of myofiber was not accelerated, but that the regeneration potential was inferior. These results clearly indicate that not only utrophin expression but also regeneration potential, perhaps a satellite cell function, directly leads to the pathological condition. The identification of genes that determine the DBA/2 phenotype will provide new therapeutic strategies for the treatment of muscular dystrophy.

Acknowledgment

We thank Katherine Ono for reading this manuscript.

References

1. Koenig M, Monaco AP, Kunkel LM: The complete sequence of dystrophin predicts a rod-shaped cytoskeletal protein. Cell 1988, 53:219–228
2. Suzuki A, Yoshida M, Hayashi K, Mizuno Y, Hagiwara Y, Ozawa E: Molecular organization at the glycoprotein-complex-binding site of dystrophin. Three dystrophin-associated proteins bind directly to the carboxy-terminal portion of dystrophin. Eur J Biochem 1994, 220:283–292
3. Ervasti JM, Campbell KP: A role for the dystrophin-glycoprotein complex as a transmembrane linker between laminin and actin. J Cell Biol 1993, 122:809–823
4. Carpenter S, Karpati G: Disease of skeletal muscle. Edited by S Carpenter, G Karpati. New York, Oxford University Press, Inc., 2001, pp. 373–524
5. Bulfield G, Siller WG, Wight PA, Moore KJ: X chromosome-linked muscular dystrophy (mdx) in the mouse. Proc Natl Acad Sci USA 1984, 81:1189–1192
6. Stedman HH, Sweeney HL, Shrager JB, Maguire HC, Panettieri RA, Petrof B, Narusawa M, Leferovich JM, Sladky JT, Kelly AM: The mdx mouse diaphragm reproduces the degenerative changes of Duchenne muscular dystrophy. Nature 1991, 352:536–539
7. Tanabe Y, Esaki K, Nomura T: Skeletal muscle pathology in X chromosome-linked muscular dystrophy (mdx) mouse. Acta Neuropathol 1986, 69:91–95
8. Pastoret C, Sebille A: mdx mice show progressive weakness and muscle deterioration with age. J Neurol Sci 1995, 129:97–105
9. Deconinck AE, Rafael JA, Skinner JA, Brown SC, Potter AC, Metzinger L, Watt DJ, Dickson JG, Tinsley JM, Davies KE: Utrophin-dystrophin-deficient mice as a model for Duchenne muscular dystrophy. Cell 1997, 90:717–727
10. Grady RM, Teng H, Nichol MC, Cunningham JC, Wilkinson RS, Sanes JR: Skeletal and cardiac myopathies in mice lacking utrophin and dystrophin: a model for Duchenne muscular dystrophy. Cell 1997, 90:729–738
11. Bischoff R: Analysis of muscle regeneration using single myofibers in culture. Med Sci Sports Exerc 1989, 21:S164–172
12. Mauro A: Satellite cell of skeletal muscle fibers. J Biophys Biochem Cytol 1961, 9:493–495
13. Schultz E, Gibson MC, Champion T: Satellite cells are mitotically quiescent in mature mouse muscle: an EM and radioautographic study. J Exp Zool 1978, 206:451–456
14. Collins CA, Olsen I, Zammit PS, Heslop L, Petrie A, Partridge TA, Morgan JE: Stem cell function, self-renewal, and behavioral heterogeneity of cells from the adult muscle satellite cell niche. Cell 2005, 122:289–301
15. Luz MA, Marques MJ, Santo Neto H: Impaired regeneration of dystrophin-deficient muscle fibers is caused by exhaustion of myogenic cells. Braz J Med Biol Res 2002, 35:691–695
16. Amalfitano A, Chamberlain JS: The mdx-amplification-resistant mutation system assay, a simple and rapid polymerase chain reaction-based detection of the mdx allele. Muscle Nerve 1996, 19:1549–1553
17. Fukada S, Yamamoto Y, Segawa M, Sakamoto K, Nakajima M, Sato M, Morikawa D, Uezumi A, Miyagoe-Suzuki Y, Takeda S, Tsujikawa K, Yamamoto H: CD90-positive cells, an additional cell population, produce laminin alpha2 upon transplantation to dy(3k)/dy(3k) mice. Exp Cell Res 2008, 314:193–203
18. Fukada S, Higuchi S, Segawa M, Koda K, Yamamoto Y, Tsujikawa K, Kohama Y, Uezumi A, Imamura M, Miyagoe-Suzuki Y, Takeda S, Yamamoto H: Purification and cell-surface marker characterization of quiescent satellite cells from murine skeletal muscle by a novel monoclonal antibody. Exp Cell Res 2004, 296:245–255
19. Matsuda R, Nishikawa A, Tanaka H: Visualization of dystrophic muscle fibers in mdx mouse by vital staining with Evans blue: evidence of apoptosis in dystrophin-deficient muscle. J Biochem 1995, 118:959–964
20. Handschin C, Chin S, Li P, Liu F, Maratos-Flier E, Lebrasseur NK, Yan Z, Spiegelman BM: Skeletal muscle fiber-type switching, exercise intolerance, and myopathy in PGC-1alpha muscle-specific knock-out animals. J Biol Chem 2007, 282:30014–30021
21. Seale P, Sabourin LA, Girgis-Gabardo A, Mansouri A, Gruss P, Rudnicki MA: Pax7 is required for the specification of myogenic satellite cells. Cell 2000, 102:777–786
22. Connolly AM, Keeling RM, Mehta S, Pestronk A, Sanes JR: Three mouse models of muscular dystrophy: the natural history of strength and fatigue in dystrophin-, dystrophin/utrophin-, and laminin alpha2-deficient mice. Neuromuscul Disord 2001, 11:703–712
23. Charge SB, Rudnicki MA: Cellular and molecular regulation of muscle regeneration. Physiol Rev 2004, 84:209–238
24. Sacco A, Doyonnas R, Kraft P, Vitorovic S, Blau HM: Self-renewal and expansion of single transplanted muscle stem cells. Nature 2008, 456:502–506
25. Sadeh M, Czyewski K, Stern LZ: Chronic myopathy induced by repeated bupivacaine injections. J Neurol Sci 1985, 67:229–238
26. Arnold L, Henry A, Poron F, Baba-Amı Y, van Rooijen N, Plonquet A, Gherardi RK, Chazaud B: Inflammatory monocytes recruited after skeletal muscle injury switch into anti-inflammatory macrophages to support myogenesis. J Exp Med 2007, 204:1057–1069
27. Segawa M, Fukada S, Yamamoto Y, Yahagi H, Kanematsu M, Sato M, Ito T, Uezumi A, Hayashi S, Miyagoe-Suzuki Y, Takeda S, Tsujikawa K, Yamamoto H: Suppression of macrophage functions impairs skeletal muscle regeneration with severe fibrosis. Exp Cell Res 2008, 314:3232–3244
28. Grounds MD, McGeachie JK: A comparison of muscle precursor replication in crush-injured skeletal muscle of Swiss and BALBc mice. Cell Tissue Res 1989, 255:385–391
29. Gelman R, Watson A, Bronson R, Yunis E: Murine chromosomal regions correlated with longevity. Genetics 1988, 118:693–704
30. Lionikas A, Blizard DA, Vandenbergh DJ, Stout JT, Vogler GP, McClearn GE, Larsson L: Genetic determinants of weight of fast- and slow-twitch skeletal muscles in old mice. Mamm Genome 2006, 17:615–628
31. Heydemann A, Huber JM, Demonbreun A, Hadhazy M, McNally EM: Genetic background influences muscular dystrophy. Neuromuscul Disord 2005, 15:601–609
32. Manning EL, Crossland J, Dewey MJ, Van Zant G: Influences of

inbreeding and genetics on telomere length in mice. Mamm Genome 2002, 13:234–238
33. Kuang S, Kuroda K, Le Grand F, Rudnicki MA: Asymmetric self-renewal and commitment of satellite stem cells in muscle. Cell 2007, 129:999–1010
34. Schultz E, Lipton BH: Skeletal muscle satellite cells: changes in proliferation potential as a function of age. Mech Ageing Dev 1982, 20:377–383
35. Dykstra B, de Haan G: Hematopoietic stem cell aging and self-renewal. Cell Tissue Res 2008, 331:91–101
36. Chen J, Astle CM, Harrison DE: Genetic regulation of primitive hematopoietic stem cell senescence. Exp Hematol 2000, 28:442–450
37. Liang Y, Jansen M, Aronow B, Geiger H, Van Zant G: The quantitative trait gene latexin influences the size of the hematopoietic stem cell population in mice. Nat Genet 2007, 39:178–188
38. Sicinski P, Geng Y, Ryder-Cook AS, Barnard EA, Darlison MG, Barnard PJ: The molecular basis of muscular dystrophy in the mdx mouse: a point mutation. Science 1989, 244:1578–1580
39. Gargioli C, Coletta M, De Grandis F, Cannata SM, Cossu G: PlGF-MMP-9-expressing cells restore microcirculation and efficacy of cell therapy in aged dystrophic muscle. Nat Med 2008, 14:973–978
40. Muntoni F, Mateddu A, Marchei F, Clerk A, Serra G: Muscular weakness in the mdx mouse. J Neurol Sci 1993, 120:71–77
41. Hara H, Nolan PM, Scott MO, Bucan M, Wakayama Y, Fischbeck KH: Running endurance abnormality in mdx mice. Muscle Nerve 2002, 25:207–211
42. Carter GT, Wineinger MA, Walsh SA, Horasek SJ, Abresch RT, Fowler WM, Jr.: Effect of voluntary wheel-running exercise on muscles of the mdx mouse, Neuromuscul Disord 1995, 5:323–332
43. Lynch GS, Hinkle RT, Chamberlain JS, Brooks SV, Faulkner JA: Force and power output of fast and slow skeletal muscles from mdx mice 6–28 months old. J Physiol 2001, 535:591–600
44. Chamberlain JS, Metzger J, Reyes M, Townsend D, Faulkner JA: Dystrophin-deficient mdx mice display a reduced life span and are susceptible to spontaneous rhabdomyosarcoma. FASEB J 2007, 21:2195–2204

Cell Metabolism

Crosstalk between Glucocorticoid Receptor and Nutritional Sensor mTOR in Skeletal Muscle

Noriaki Shimizu,[1,10] Noritada Yoshikawa,[1,2,10] Naoki Ito,[3,4] Takako Maruyama,[1] Yuko Suzuki,[3] Sin-ichi Takeda,[3] Jun Nakae,[5] Yusuke Tagata,[9] Shinobu Nishitani,[9] Kenji Takehana,[9] Motoaki Sano,[6] Keiichi Fukuda,[6] Makoto Suematsu,[7,8] Chikao Morimoto,[1,2] and Hirotoshi Tanaka[1,2,*]

[1]Division of Clinical Immunology, Advanced Clinical Research Center
[2]Department of Rheumatology and Allergy, Research Hospital
Institute of Medical Science, University of Tokyo, Tokyo 108-8639, Japan
[3]Department of Molecular Therapy, National Institute of Neuroscience, National Center of Neurology and Psychiatry, Kodaira 187-8502, Japan
[4]Department of Biological Information, Tokyo Institute of Technology, Yokohama 226-8501, Japan
[5]Frontier Medicine on Metabolic Syndrome, Division of Endocrinology, Metabolism and Nephrology, Department of Internal Medicine
[6]Cardiology Division, Department of Internal Medicine
[7]Department of Biochemistry
[8]JST ERATO, Suematsu Gas Biology Project
Keio University School of Medicine, Tokyo 160-8582, Japan
[9]Ajinomoto Pharmaceuticals Co., Ltd., Kawasaki 210-8681, Japan
[10]These authors contributed equally to this work
*Correspondence: hirotnk@ims.u-tokyo.ac.jp
DOI 10.1016/j.cmet.2011.01.001

SUMMARY

Maintenance of skeletal muscle mass relies on the dynamic balance between anabolic and catabolic processes and is important for motility, systemic energy homeostasis, and viability. We identified direct target genes of the glucocorticoid receptor (GR) in skeletal muscle, i.e., REDD1 and KLF15. As well as REDD1, KLF15 inhibits mTOR activity, but via a distinct mechanism involving BCAT2 gene activation. Moreover, KLF15 upregulates the expression of the E3 ubiquitin ligases atrogin-1 and MuRF1 genes and negatively modulates myofiber size. Thus, GR is a liaison involving a variety of downstream molecular cascades toward muscle atrophy. Notably, mTOR activation inhibits GR transcription function and efficiently counteracts the catabolic processes provoked by glucocorticoids. This mutually exclusive crosstalk between GR and mTOR, a highly coordinated interaction between the catabolic hormone signal and the anabolic machinery, may be a rational mechanism for fine-tuning of muscle volume and a potential therapeutic target for muscle wasting.

INTRODUCTION

Muscle comprises ~40% of body mass and contributes not only to the structure and movement of the body but also to nutrient storage and supply (Matthews, 1999). In adult mammals, skeletal muscle hypertrophy/atrophy is characterized by an increase/decrease in the size (as opposed to the number) of individual myofibers, respectively. The control of muscle mass is believed to be determined by a dynamic balance between anabolic and catabolic processes (Hoffman and Nader, 2004). Mammalian target of rapamycin (mTOR) is a crucial component of the anabolic machinery for protein synthesis. mTOR consists of two complexes: mTORC1, which includes Raptor, signals to S6K and 4E-BP1, controls protein synthesis, and is rapamycin sensitive; and mTORC2, which includes Rictor, signals to Akt, and is rapamycin insensitive. mTORC1 integrates four major signals: growth factors, energy status, oxygen, and amino acids, especially branched-chain amino acids (BCAAs). Prototypically, insulin/IGF-1 activates mTOR via the PI3K-Akt pathway (Sengupta et al., 2010). It is currently considered that mTORC1, and not mTORC2, is essential for the maintenance of muscle mass and function (Bentzinger et al., 2008; Risson et al., 2009). Protein degradation in skeletal muscle cells is essentially mediated by the activity of two conserved pathways: the ubiquitin-proteasomal pathway and the autophagic/lysosomal pathway (Sandri, 2008). The ubiquitin-proteasomal pathway is responsible for the turnover of the majority of soluble and myofibrillar muscle proteins. The activity of this pathway is markedly increased in atrophying muscle due to the transcriptional activation of a set of E3 ligase-encoding genes, e.g., atrogin-1 and MuRF1 (Glass, 2003; Sandri et al., 2004). Autophagy also plays an important role in the degradation of skeletal muscle, and is indicated to be a consequence of an ordered transcriptional program involving a battery of genes, e.g., LC3 and Bnip3 (Mizushima et al., 2008). These positive and negative pathways are balanced in a highly coordinated manner for the determination of myofiber size and total muscle volume; however, distortion of this balance with a relative increase in degradation results in the generalized decrease of myofiber size and muscle atrophy (Hoffman and Nader, 2004). Pioneering studies demonstrated that muscle atrophy is a result of active processes that are transcriptionally controlled through the expression of a particular gene set; the forkhead box O (FoxO) transcription factors are

common components of a number of atrophy models and act as critical liaison molecules for protein degradation and autophagy via the transcriptional regulation of, for example, atrogin-1, MuRF1, LC3, and Bnip3 (Mammucari et al., 2007; Sandri et al., 2004; Stitt et al., 2004; Zhao et al., 2007). In clear contrast, it is evident that each disease has proper signaling pathways to FoxOs and that other components of the cellular machinery often participate in the progression of atrophy (Moresi et al., 2010; Suzuki et al., 2007). Therefore, for the development of therapies against muscle atrophy, it should be addressed how the transcriptional program triggered by a particular atrophy pathway is orchestrated and how the balance of muscle protein synthesis and degradation is distorted in each disease.

Adrenal glucocorticoids produce their actions via a signal pathway involving the ubiquitously expressed glucocorticoid receptor (GR), a prototypic member of the nuclear receptor superfamily, which acts as a ligand-dependent transcription factor. Upon binding glucocorticoids, GR translocates into the nucleus and binds to the glucocorticoid response element (GRE) in the promoters of target genes. The binding of liganded receptors to target DNA is followed by the recruitment of mediators and coactivators to the proximity of GRE, resulting in the recruitment of RNA polymerase II (RNAPII) to nearby transcription start sites and the activation of transcription (Evans, 2005; Meijsing et al., 2009). In skeletal muscle, glucocorticoids elicit a variety of biological actions in the metabolism of glucose, lipids, and proteins and contribute to metabolic homeostasis (Munck et al., 1984). On the other hand, the prolonged oversecretion or exogenous administration of glucocorticoid gives rise to undesirable effects including muscle atrophy (Munck et al., 1984). Although many studies addressed the mechanism of glucocorticoid-induced muscle atrophy, how the glucocorticoid-GR system generates the functional coupling between metabolic regulation and volume adjustment in skeletal muscle remains unsolved. Of note, many pathological conditions characterized by muscle atrophy, e.g., sepsis, cachexia, starvation, metabolic acidosis, and severe insulinopenia, are associated with an increase in circulating glucocorticoid levels. Adrenalectomy or treatment with the GR antagonist RU486 attenuates muscle atrophy in sepsis, cachexia, starvation, and severe insulinopenia (Menconi et al., 2007; Schakman et al., 2008). Moreover, endogenous glucocorticoids were shown to be essential for muscle atrophy in acute diabetic rodents (Hu et al., 2009). Together, understanding the glucocorticoid-mediated regulation of metabolism-volume coupling in muscle is increasingly important for the management of not only muscle atrophy but also these wasting/metabolic disorders.

Typically, glucocorticoid-induced muscle atrophy is characterized by fast-twitch type II glycolytic muscle fiber loss with reduced or no impact on type I fibers. The mechanism of such fiber specificity is yet unknown. Previous reports suggested that the glucocorticoid-GR system has antianabolic and catabolic effects and promotes degradation via the induction of a set of genes including atrogin-1, MuRF1, and myostatin (Menconi et al., 2007; Schakman et al., 2008). Although the involvement of FoxO transcription factors is reported in the gene regulation of atrogin-1 and MuRF1 under the presence of excess glucocorticoids (Sandri et al., 2004; Stitt et al., 2004), the biochemical role of GR in the transcriptional regulation of muscle tissue has not yet been determined. Therefore, we investigated how GR-mediated gene expression coordinately modulates antianabolic and catabolic actions to understand the functional coupling of metabolism and volume regulation in muscle.

In the present study, we identified REDD1 and KLF15 genes as direct targets of GR. REDD1 is known to be induced by various stressors, including glucocorticoid, and to inhibit mTOR activity via the sequestration of 14-3-3 and the increase of TSC1/2 activity (Wang et al., 2006; DeYoung et al., 2008). We clearly identified the functional GRE via the promoter analysis of REDD1 gene. On the other hand, KLF15 is a recently discovered transcription factor that is involved in several metabolic processes in skeletal muscle; e.g., KLF15 transcriptionally upregulates the gene expression of branched-chain aminotransferase 2 (BCAT2), a mitochondrial enzyme catalyzing the first reaction in the catabolism of BCAA to accelerate BCAA degradation and alanine production in skeletal muscle (Gray et al., 2007). Moreover, phenotypic analysis of cardiac-specific KLF15 knockout mice revealed marked left ventricular hypertrophy, indicating the negative regulatory role of KLF15 on muscle mass (Fisch et al., 2007). We here demonstrated that KLF15 participates in muscle catabolism via the transcriptional regulation of atrogin-1 and MuRF1. Moreover, KLF15 affects mTOR through BCAA degradation and negatively modulates myofiber size. mTOR activation inhibits GR-mediated transcription by suppressing GR recruitment onto target genes, strongly suggesting a mutually exclusive crosstalk between mTOR and GR. Pharmacological activation of mTOR with BCAA attenuated GR-mediated gene expression, leading to the substantial restoration of muscle in glucocorticoid-treated rats. We, therefore, indicate the critical importance of the interaction of GR and mTOR in the regulation of metabolism-volume coupling in skeletal muscle.

RESULTS

REDD1 and KLF15 Are Target Genes of GR in Skeletal Muscle

GR levels were relatively high in type II-rich gastrocnemius and tibialis anterior muscles compared to type I-rich soleus muscle in rats (Figure 1A). Figure 1B illustrates the comparison of the effects of a 3 hr treatment with dexamethasone (DEX) on mRNA expression of various genes between the gastrocnemius and soleus muscles. Hormonal induction of mRNA expression of REDD1, atrogin-1, MuRF1, KLF15, FoxO1, FoxO3, and myostatin, as well as the well-known GR target gene FKBP5 (Yoshikawa et al., 2009), was observed in both muscles, but to a lesser extent in the soleus muscle. Among the genes induced by DEX at 3 hr (Figure 1B), the promoter regions of MuRF1 (Waddell et al., 2008) and myostatin (Ma et al., 2001), but not atrogin-1 (Sandri et al., 2004), contain functional GREs. In addition, REDD1 and KLF15 were also considered as candidates of GR target genes (see the Supplemental Information available online).

Concerning KLF15, we showed, in gastrocnemius muscle and L6 myotubes but not in liver, that KLF15 mRNA and protein expression was induced in a GR-dependent manner (Figure 2A). The promoter region spanning from −4676 to +116 of KLF15 gene was not responsive to DEX; however, the activity of the region spanning −2108 to +1331 was induced by DEX, and

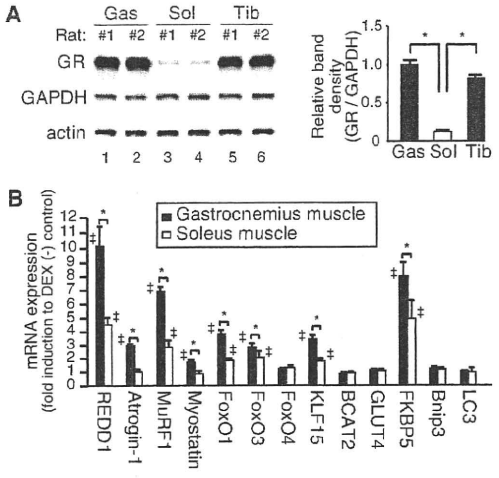

Figure 1. GR Protein Expression and Glucocorticoid-Dependent mRNA Expression of Atrophy-Related Genes in Rat Skeletal Muscles

(A) GR protein levels in rat gastrocnemius (Gas), soleus (Sol), and tibialis anterior (Tib). Left, representative immunoblots. Right, quantified protein levels of GR relative to GAPDH (n = 9).

(B) Induction of mRNA levels of atrophy-related genes by dexamethasone (DEX). Expression levels of the indicated mRNA in the muscles from rats 3 hr after intraperitoneal injection with DEX were assessed in quantitative RT-PCR (qRT-PCR). Results are shown as fold induction to vehicle-treated rats (n = 6).

(A and B) Error bars show SD. *$p < 0.05$, ‡$p < 0.05$ versus vehicle-treated rats.

this induction was inhibited by a GR antagonist RU486. The deletion and mutational analyses of KLF15 promoter indicated that both upper GRE1 and lower GRE2 sites were functional (Figures 2B and 2C). The transient transfection assays using the reporter constructs conveying these minimal GRE sites clearly showed that each GRE is independently functional (Figure 2D). A chromatin immunoprecipitation (ChIP) assay revealed that both GRE-like sequences were targeted by GR and that RNAPII was incorporated onto the coding region of KLF15 gene in the presence of DEX in L6 cells (Figure 2E). We also confirmed the DEX-dependent recruitment of endogenous GR onto the KLF15 promoter in a skeletal muscle-specific manner in vivo (Figure 2F). Similarly, we identified the functional GRE on the REDD1 promoter region and confirmed REDD1 as a GR target gene as well (Figure S1).

KLF15 Transactivates atrogin-1 and MuRF1 Genes

Next, we studied the alteration in the gene expression profile after the direct injection of a KLF15-expressing adenovirus into the rat tibialis anterior muscle. The exogenous expression of KLF15 increased KLF15 protein levels by approximately 5-fold (Figure 3A) and significantly induced mRNA expression of its target gene BCAT2 as anticipated (Figure 3B). Moreover, mRNA expression of atrogin-1, MuRF1, FoxO1, and FoxO3 was stimulated by KLF15 (Figure 3B). We then focused on atrogin-1 and MuRF1 and asked whether the DEX-mediated induction of their mRNA expression was dependent on KLF15. For that purpose, we tested the effect of knocking down the expression of GR or KLF15 on mRNA expression of KLF15, atrogin-1, and MuRF1 as well as another GR target gene REDD1 as a control. In L6 myoblasts, GR knockdown diminished the DEX-dependent mRNA induction of all of these GR target genes. However, KLF15 knockdown affected that of atrogin-1 and MuRF1 but not REDD1 (Figure 3C). These results strongly indicate the critical involvement of the GR-KLF15 cascade in the DEX-mediated upregulation of atrogin-1 and MuRF1 gene expression. To address the role of KLF15 in the transcriptional regulation of atrogin-1 and MuRF1, we constructed luciferase reporter plasmids driven by the promoter of rat atrogin-1 or MuRF1, and tested the effect of the exogenous expression of KLF15 in L6 myoblasts. The expression of the reporter genes was upregulated in a KLF15-dependent manner (Figure 3D). Since the promoter regions of atrogin-1 and MuRF1 contain a number of putative KLF15 recognition sites, we performed ChIP analyses; both promoters had multiple KLF15 binding sites and some of them were located in the proximity of FoxO binding sites and GRE (Figure 3E), and at least one of these KLF15 sites of each promoter recruited KLF15 in a DEX-dependent manner in vivo as well (Figure 3F). Note that atrogin-1 and MuRF1 were originally identified as FoxO target genes (Sandri et al., 2004; Waddell et al., 2008) and that KLF15 induced FoxO mRNA expression (Figure 3B). Indeed, the combination of KLF15 and FoxO significantly enhanced the promoter activity of atrogin-1 and MuRF1 when compared to their individual effects (Figure 3G). Moreover, the direct injection of the adenovirus expressing constitutively active FoxO1 or KLF15 significantly increased atrogin-1 and MuRF1 mRNA expression, and the expression of both resulted in synergistic or additive effects in tibialis anterior (Figure 3H). Therefore, it is likely that KLF15 and FoxO transcription factors cooperatively upregulate the expression of atrogin-1 and MuRF1 genes.

GR-KLF15 Axis Modulates BCAA Metabolism and mTOR Activity

Next, we studied the effects of glucocorticoids, GR, and KLF15 on BCAT2 and BCAA catabolism in skeletal muscle cells. In gastrocnemius muscle, mRNA expression of KLF15 preceded that of BCAT2 after treatment with DEX (Figure 4A). Overexpression of KLF15 increased the BCAT2 promoter-luciferase reporter activity (Figure 4B). Moreover, DEX-induced BCAT2 promoter activation was inhibited by either RU486 or siKLF15 (Figure 4C), indicating that KLF15 is mandatory for GR-mediated BCAT2 gene activation. BCAT2 enzyme activity was stimulated by DEX, and this effect was abolished in the presence of RU486 (Figure 4D). In tibialis anterior muscle and L6 myotubes, the adenovirus-mediated exogenous expression of KLF15 significantly induced BCAT2 enzyme activity even in the absence of DEX (Figure 4E).

The measurement of intracellular amino acid levels clearly revealed the accelerated catabolism of BCAA by KLF15 in myotubes; the exogenous expression of KLF15 decreased the levels of Val, Leu, and Ile, with a reciprocal increase in Ala and Glu without significant alterations in, for example, Gly, Trp, Gln, Tyr, and Phe, in L6 myotubes (Figure 4F). Amino acids, especially BCAA, are believed to activate mTOR and to increase in association with Rheb-mTOR (Sancak et al., 2010). We showed that overexpression of KLF15 in C2C12 myotubes suppressed mTOR activity as demonstrated by the decrease in the phosphorylated form of S6K1. Moreover, mTOR activity was complemented by the addition of excess BCAA (Figure 4G). Of note,

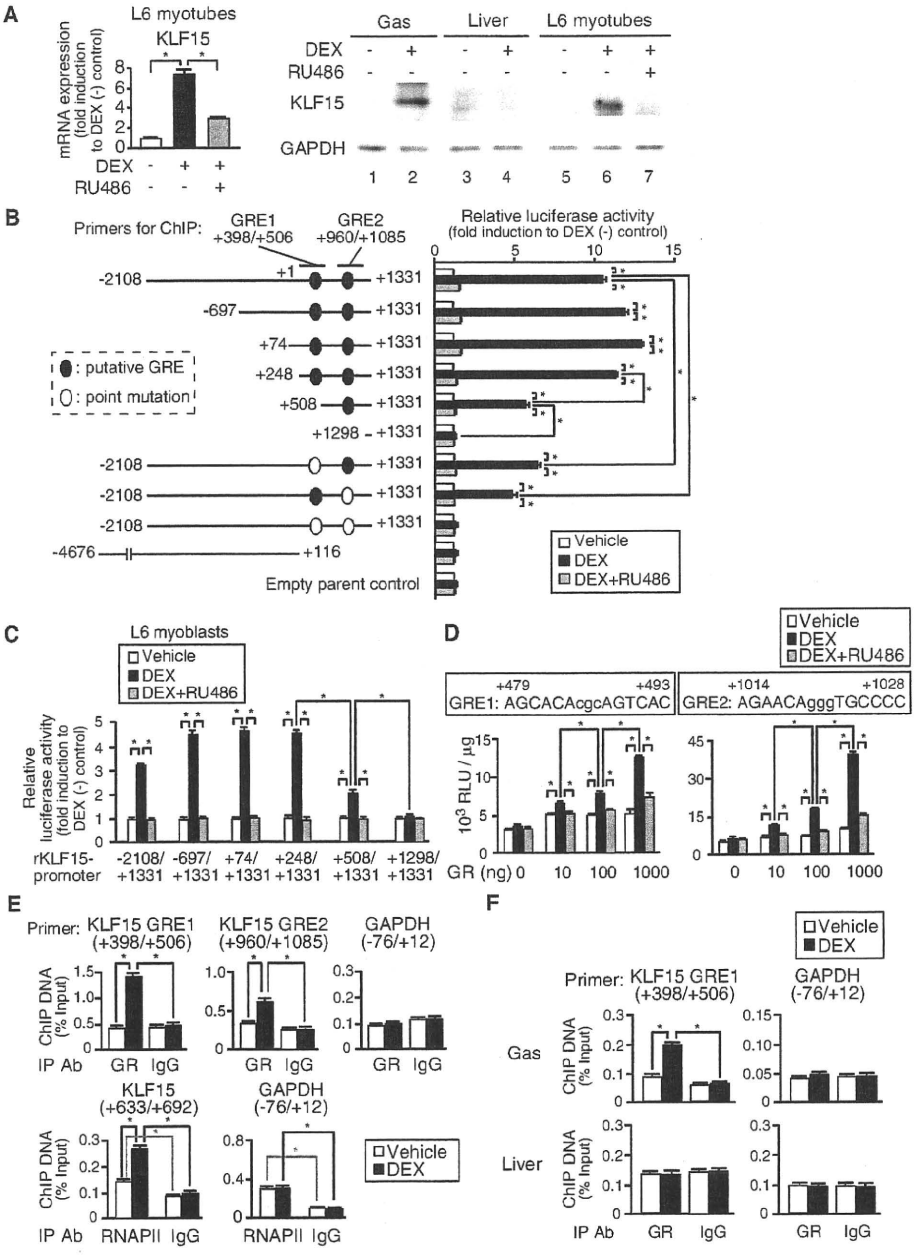

Figure 2. Identification of KLF15 as a Direct GR Target Gene

(A) GR-dependent mRNA (left) and protein (right) expression of KLF15 in L6 myotubes treated with DEX and RU486 for 6 hr and in DEX-treated rat gastrocnemius (see legend for Figure 1B).

(B) Identification of GREs in rat KLF15 promoter. Left, schematic of rat KLF15 promoter-luciferase reporter constructs. Positions of the primers for chromatin immunoprecipitation (ChIP) in (E) and (F) are shown. Right, GR-dependent activation of rat KLF15 promoter-reporter genes. COS-7 cells were transfected with the reporter constructs and 100 ng of GR expression plasmid and treated with DEX and RU486 for 18 hr.

(C) GR-dependent activation of rat KLF15 promoter-reporter genes in L6 myoblasts treated with DEX and RU486 for 18 hr.

(D) GR-dependent activation of reporter genes containing KLF15 promoter GREs. L6 myoblasts were transfected with the luciferase reporter constructs containing the GREs from rat KLF15 with GR expression plasmid and treated with DEX and RU486 for 18 hr.

(E) DEX-dependent recruitment of GR and RNAPII onto rat KLF15 gene. L6 myotubes treated with 1 µM DEX for 2 hr were subjected to ChIP.

(F) Skeletal muscle-specific recruitment of GR onto rat KLF15 gene by DEX. DEX-treated rat gastrocnemius (Gas) and liver (see legend for Figure 1B) were subjected to ChIP.

(A–F) Error bars show SD (n = 5). *p < 0.05.

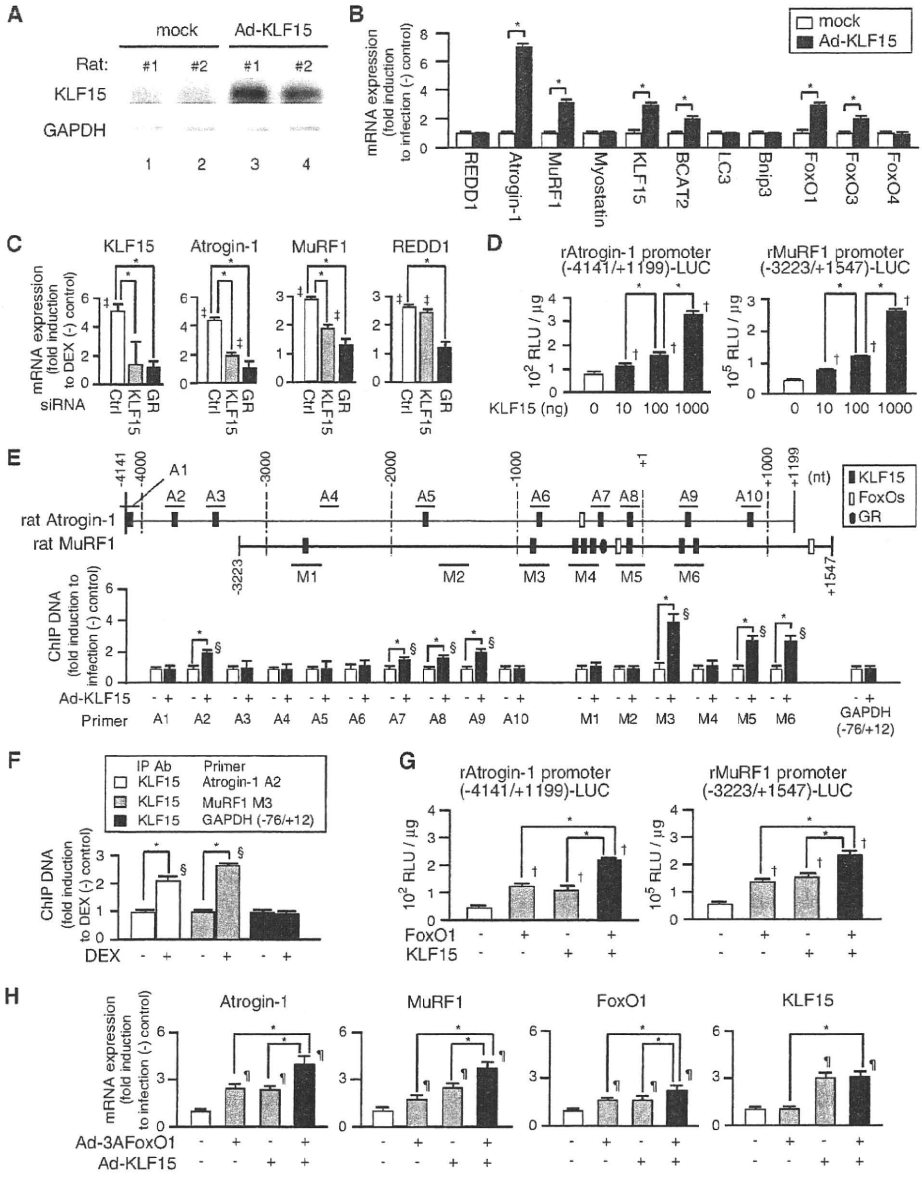

Figure 3. Transcriptional Regulation of Atrogenes by KLF15 and FoxOs

(A and B) KLF15-dependent mRNA expression of atrophy-related genes. Recombinant adenovirus Ad-KLF15 was infected to rat tibialis anterior for 7 days. (A) Immunoblot detection of ectopic KLF15. (B) qRT-PCR.

(C) Effects of knockdown of KLF15 or GR on DEX-dependent mRNA expression of atrophy-related genes. L6 myoblasts were transfected with control siRNA, siRNA against KLF15, or siRNA against GR and treated with DEX for 18 hr.

(D) KLF15-dependent activation of rat atrogin-1 (left) and MuRF1 (right) promoter-reporter genes in L6 myoblasts.

(E) Mapping of the binding sites for KLF15, FoxOs, and GR in rat atrogin-1 and MuRF1 promoters. Top, putative binding sites identified in in silico promoter analysis (see the Experimental Procedures and the Supplemental Information). Bars indicate the positions of the primers for ChIP. Bottom, recruitment of KLF15 onto rat atrogin-1 and MuRF1 promoters. L6 myotubes were infected with Ad-KLF15 for 5 days and subjected to ChIP using anti-KLF15 antibody.

(F) DEX-dependent recruitment of KLF15 onto rat atrogin-1 and MuRF1 promoters in rat gastrocnemius (see Figure 1B).

(G and H) Effects of FoxOs and KLF15 on rat atrogin-1 and MuRF1 promoter-reporter gene expression in L6 myoblasts (G) and on atrogin-1 and MuRF1 mRNA expression in rat tibialis anterior (H). (G) Luciferase assay of L6 myoblasts transfected with the reporter constructs with or without FoxO1 and/or KLF15 expression plasmids. (H) qRT-PCR analysis of rat tibialis anterior expressing ectopic KLF15 and/or constitutive active FoxO1 (3AFoxO1) for 3 days.

(B–H) Error bars show SD (n = 5). *$p < 0.05$, †$p < 0.05$ versus vehicle-treated cells, ‡$p < 0.05$ versus mock-transfected cells, §$p < 0.05$ versus ChIP with normal IgG, ¶$p < 0.05$ versus mock-infected rats.

the diameter of C2C12 myotubes was shortened by KLF15 and rescued by BCAA (Figure 4G). Moreover, exogenous KLF15 reduced mTOR activity with fiber type-independent atrophy in the tibialis anterior muscle (Figure 4H). Taken together, these data indicate that KLF15 is a liaison molecule for GR in the induction of atrogenes and the acceleration of BCAA catabolism and mTOR repression to decrease myofiber size.

mTOR Affects GR-Mediated Transcriptional Regulation

Since little is known about how glucocorticoid-mediated catabolic signal transduction is shut off, we next examined the effects of mTOR blockade using rapamycin on GR-mediated gene expression in L6 myotubes. Surprisingly, rapamycin significantly enhanced the DEX-induced mRNA expression of a number of GR target genes, including REDD1, atrogin-1, MuRF1, KLF15, FoxOs, and FKBP5 (Figure 5A). These results strongly suggest that mTOR blockade selectively enhances mRNA expression of GR target genes, i.e., mTOR activation appears to have a negative impact on GR-mediated gene expression. To further address this negative modulation of GR function by mTOR, we performed transient transfection assays using GR-responsive KLF15 promoter-Luc and GRE-Luc reporter genes in L6 myoblasts. A constitutively active mutant of Rheb, RhebS16H, which autonomously activates mTOR, repressed DEX-mediated reporter gene activation, and rapamycin inhibited these negative effects of RhebS16H (Figure 5B). Moreover, a major endogenous mTOR activator IGF-1 slightly enhanced S6K1 phosphorylation and did not affect DEX-induced GRE-Luc expression when cultured in amino acid-rich media. In clear contrast, in amino acid-deprived media, DEX-dependent induction of GRE-Luc was approximately doubled, and IGF-1 strongly phosphorylated S6K1 and suppressed DEX-induced GRE-Luc expression (Figure 5C). These results indicated that, regardless of the upstream pathways for mTOR activation, endogenous GR activity is negatively controlled by mTOR in L6 myoblasts.

We then asked the underlying mechanisms for mTOR-mediated GR suppression. To test whether mTOR-mediated GR repression is via global protein synthesis downstream of mTOR, we examined luciferase mRNA expression in transient transfection assay using GRE-Luc reporter plasmid in the presence or absence of the protein synthesis inhibitor cycloheximide. Cycloheximide did not influence on either GR-mediated GRE activation or BCAA-mediated GR suppression (Figure 5D). Therefore, BCAA inhibits the transcriptional effects of GR via mTOR activation but not via de novo protein synthesis. Immunoblotting using L6 myotubes revealed that GR protein levels were unaltered in the presence of DEX, BCAA, or rapamycin. Treatment with DEX clearly promoted the nuclear translocation of GR, and such a process was not affected by BCAA or rapamycin (Figure 5E). Concerning the promoter regions spanning the putative GREs in KLF15 and REDD1, DEX-induced GR recruitment was significantly enhanced by rapamycin, suggesting that mTOR negatively influences the access of GR to these promoters. Such an enhancement of GR promoter binding by rapamycin was paralleled by RNAPII recruitment onto the coding regions of KLF15 and REDD1 (Figure 5F). Thus, cellular mTOR activity negatively modulates GR transcriptional function, most possibly by altering the intranuclear behavior of GR. We finally examined the effect of constitutive mTOR activation by studying the impact of adeno-associated virus-driven RhebS16H expression on S6K1 activity and the gene expression profile of the tibialis anterior muscle from DEX-treated rats. RhebS16H-injected muscle had elevated levels of S6K1 phosphorylation and significant decreases in the induction response to DEX of a number of glucocorticoid-inducible genes, including REDD1, atrogin-1, MuRF1, FoxOs, KLF15, and FKBP5, when compared to mock-injected muscle (Figures 5G and 5H).

mTOR Activation Attenuates Glucocorticoid-Induced Muscle Atrophy

It should be noted that numerous studies examined the effects of BCAA on mTOR activity in glucocorticoid-induced atrophy models with conflicting results, the reason for which might be variations in the protocols used in those in vivo studies (Menconi et al., 2007; Schakman et al., 2008). We showed that the bolus administration of a BCAA cocktail via a gastric tube just before the peritoneal injection of DEX (Supplemental Information) resulted in sufficient and reproducible mTOR activation in the gastrocnemius muscle; the phosphorylated form of S6K1 was increased at 30 min after BCAA administration and returned to the baseline level after 90–180 min, even in the presence of DEX (Figure 6A). We then tested the effects of DEX, BCAA, and rapamycin on the protein levels and phosphorylation status of mTOR and its downstream effectors S6K1 and 4E-BP1 as well as Akt, the upstream activator of mTOR, in the rat glucocorticoid-induced atrophy model (5 day intraperitoneal DEX administration, see the Supplemental Information). In GR-rich gastrocnemius muscle, treatment with DEX suppressed the phosphorylation of S6K1 and 4E-BP1, without a significant alteration in p-Akt, indicating that DEX inhibited mTOR function in an Akt-independent fashion in this model. In clear contrast, in either the soleus muscle or liver, DEX treatment did not affect mTOR activity. When BCAA was supplemented, the levels of p-S6K1 and p-4E-BP1 were efficiently restored. Of note, rapamycin canceled these effects of BCAA (Figure 6B). In this model, BCAA administration suppressed the glucocorticoid-induced expression of REDD1, atrogin-1, MuRF1, KLF15, FoxOs, and FKBP5 mRNA (Figure 6C), and there was a decrease in GR recruitment onto the promoters of KLF15, REDD1, MuRF1, and FKBP5 (Figure 6D). BCAA administration also repressed the expression of BCAT2, GLUT4, Bnip3, and LC3 mRNA, and treatment with rapamycin inhibited the effects of BCAA (Figure 6C). In contrast, in the soleus muscle, treatment with DEX alone or DEX plus BCAA only marginally influenced mTOR activity and the gene expression profile, if at all (Figures 6B and 6C).

In this glucocorticoid-induced muscle atrophy rat model, there was a decrease in the body weight of the DEX, DEX plus BCAA, and DEX plus BCAA plus rapamycin groups (Figure 7A). The DEX plus BCAA group revealed a significant restoration of muscle strength as determined by a grip test and the weight of the gastrocnemius muscle when compared with DEX group (Figures 7B and 7C). Histological examination of the gastrocnemius muscle demonstrated typical type II fiber-dominant atrophy in the DEX group; however, the DEX plus BCAA group showed less impairment in the gastrocnemius muscle that was represented by the prevention of type II fiber loss. Semiquantitative analysis using cross-sectional area (CSA) analysis of myofibers strongly supported this notion; the leftward shift in myofiber size

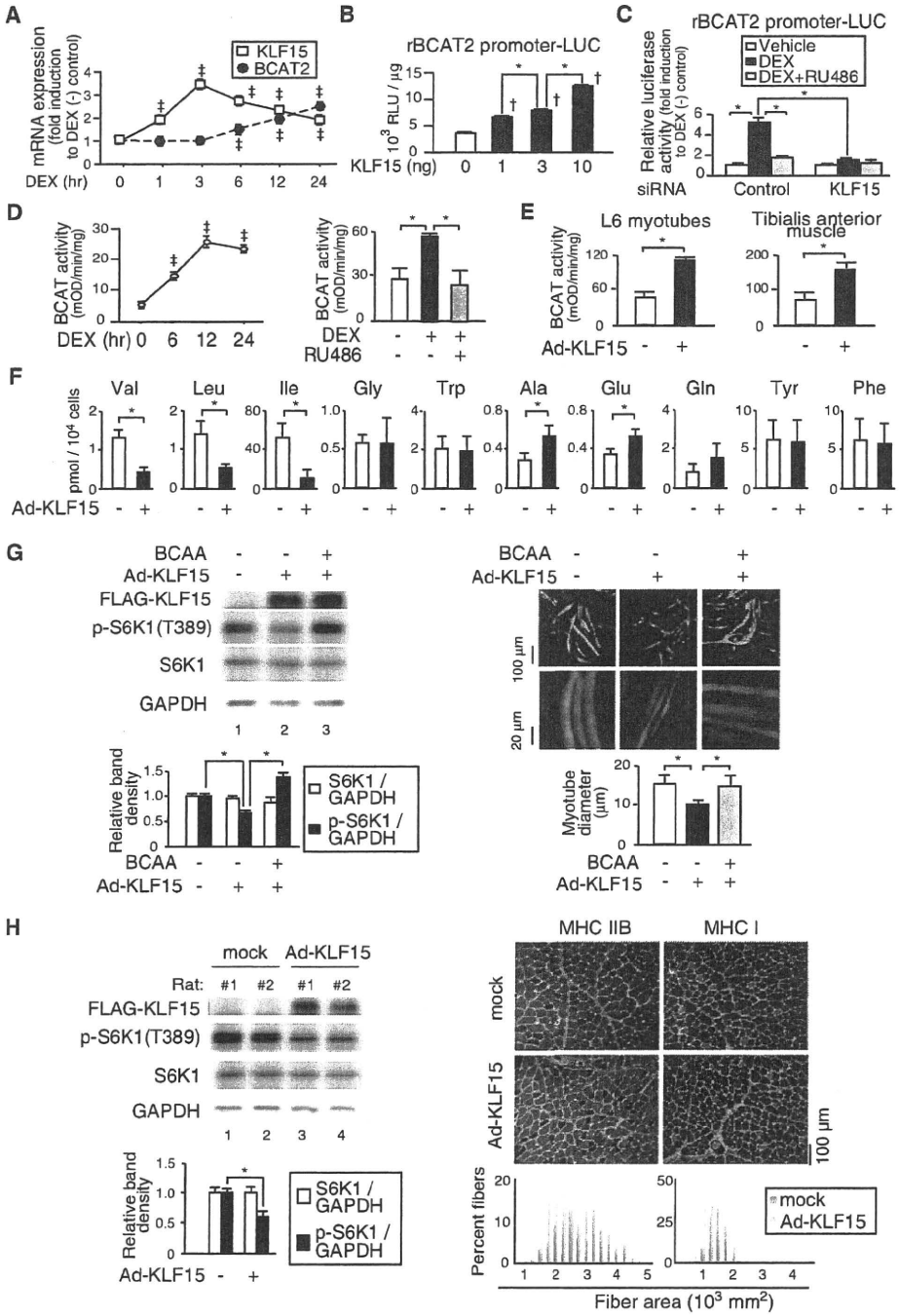

Figure 4. KLF15-Mediated Modulation of BCAA Metabolism and Myofiber Size

(A) Time course of mRNA expression of KLF15 and BCAT2 in rat gastrocnemius after intraperitoneal DEX-injection (n = 5).

(B) KLF15-dependent activation of rat BCAT2 promoter-reporter gene expression in L6 myoblasts (n = 5).

(C) Diminished GR-dependent activation of rat BCAT2 promoter-reporter gene by knockdown of KLF15 in L6 myoblasts (n = 5).

(D) GR-dependent activation of BCAT activity in rat gastrocnemius. Rats were treated with RU486 and/or DEX for the indicated time periods (left) or 6 hr (right) and subjected to BCAT activity measurement as described in the Supplemental Information (n = 5).

(E) KLF15-dependent activation of BCAT activity (n = 5).

(F) Effects of ectopic KLF15 on intracellular amino acid concentrations. L6 myotubes were infected with Ad-KLF15 for 2 days, cultured in amino acid-deprived DMEM for 24 hr, and subjected to quantification of intracellular amino acids as described in the Supplemental Information (n = 3).

(G) Effects of KLF15 and BCAA on mTOR activity and myotube diameter. C2C12 myotubes were infected with GFP-expressing adenovirus and Ad-KLF15 for 2 days and further cultured in amino acid-deprived DMEM supplemented with or without 10 mM BCAA cocktail for 24 hr. Left, representative immunoblots

was observed in the DEX group, but not in the DEX plus BCAA group. In contrast, there was no significant difference in the size of slow type I fibers among the three treatment groups. Moreover, the therapeutic effects of BCAA were inhibited by rapamycin (Figures 7B–7E). Therefore, we conclude that the administration of BCAA elicits mTOR activation and intervenes in GR-dependent catabolic transcriptional regulation to ameliorate DEX-induced muscle atrophy.

DISCUSSION

In skeletal muscle, we suggested that GR activates a secondary transcription network driven by KLF15; that the promoter regions of atrogin-1 and MuRF1 contain KLF15 binding sites as well as those of FoxOs; and that KLF15 induces the expression of these atrogenes. Although the molecular mechanism remains elusive, the functional cooperativity of GR, FoxOs, and KLF15 in the expression of the atrogenes may represent the molecular basis for the involvement of GR in muscle atrophy associated with a number of pathological conditions including diabetes and sepsis. From the metabolic viewpoint, these GR-driven transcriptional cascades appear to be relevant for providing rapid and integrated cues toward muscle breakdown and nutrient supply from muscle to other organs, i.e., to the liver, under stressful conditions associated with excess levels of glucocorticoids.

BCAT2 catalyzes the initial step for BCAA degradation, and BCAT2 activity is a critical determinant of cellular BCAA content in skeletal muscle; mice with systemic inactivation of BCAT2 gene are reported to have approximately ten times or higher concentrations of plasma BCAA (She et al., 2007). We demonstrated that BCAA content was decreased with a reciprocal increase in alanine levels in L6 myotubes after the exogenous expression of KLF15 (Figure 4F). Although it is generally known that BCAA is supplied via protein breakdown during skeletal muscle atrophy (Wagenmakers, 1998; Yu et al., 2010), it was reported that net increase in muscle BCAA concentrations after glucocorticoid treatment (~150% increase compared to control) were strikingly lower than those of diabetic rats (~400% increase compared to control) (Aftring et al., 1988; Hundal et al., 1991). This difference in BCAA concentrations is most likely to be due to increased BCAT2 activity in glucocorticoid-treated rats. The glucocorticoid-driven GR-KLF15-BCAT2 axis may negatively modulate the intracellular availability of BCAA and result in a negative impact on mTOR function in skeletal muscle. Indeed, exogenous KLF15 increased mRNA expression of the atrogenes and BCAT2 and decreased mTOR activity and BCAA concentrations in cultured myotubes (Figures 4E–4G). Moreover, the introduction of KLF15 decreased myofiber size in cultured myotubes and caused atrophy in the tibialis anterior muscle, even in the absence of glucocorticoids (Figures 4G and 4H). Therefore, we may conclude that KLF15 is a crucial GR target gene acting as a catabolic modulator of skeletal muscle.

In addition to the KLF15-BCAT2 axis, it should be noted that a number of glucocorticoid-induced products can repress mTOR activity in skeletal muscle cells. Among others, myostatin (Ma et al., 2001; Gilson et al., 2007) and REDD1 (Figure S1) (DeYoung et al., 2008) are direct targets of GR. Moreover, atrogin-1 was recently reported to inhibit S6K1 activity via eIF3f (Csibi et al., 2010). Therefore, it is likely that the mTOR system is negatively regulated by a variety of factors in the presence of excess glucocorticoids in a distinct fashion. Given that the glucocorticoid-GR axis is a major catabolic regulator for homeostatic control (Munck et al., 1984), this multimodal repression of mTOR via the GR axis appears to be rational. In any case, this type of negative mTOR modulation is not reported in other types of muscle atrophy, and may be a striking feature in glucocorticoid-induced muscle atrophy. Interestingly, muscle-specific inactivation of mTOR was reported to exacerbate the myopathic features of type I and type II fiber-rich muscles in a distinct fashion; type I fiber-rich muscles showed prominent dystrophic features with less impact on muscle mass and CSA compared to type II fiber-rich muscles, and a decrease in muscle mass and CSA are characteristic of type II fiber-rich muscles with less dystrophic appearance (Bentzinger et al., 2008; Risson et al., 2009). Therefore, we speculate that type II fiber-rich glycolytic muscles have an evolutionally preserved role for the storage of nutrients under the control of the glucocorticoid-GR axis and that the GR-triggered gene expression program is a purposeful and efficient compensatory mechanism for nutrient supply from those muscles.

An important question is how the GR-driven proteolytic cascades can be shut down when necessary in skeletal muscle. We clearly demonstrated that mTOR activation negatively modulated GR-mediated transcription. Given that the effect of mTOR is rapamycin sensitive, the involvement of mTORC1 is strongly indicated in this interaction. The role of the mTOR pathway in the determination of glucocorticoid sensitivity has not yet been highlighted, except in certain hematologic malignancies (Beesley et al., 2009; Gu et al., 2008; Yan et al., 2006a). It was postulated that the treatment of cultured cells with FK506 or rapamycin enhances glucocorticoid-inducible reporter gene expression, most possibly via their interaction with heat shock proteins and the promotion of the ligand-dependent nuclear entry of GR (Ning and Sanchez, 1993). In contrast, we documented that rapamycin, without any alteration in the cytoplasmic-nuclear distribution of GR, increased GR recruitment onto the promoter (Figures 5E and 5F), and these effects were not reproduced by FK506 (data not shown).

and quantified band densities of S6K1 and p-S6K1(T389) relative to GAPDH (n = 5). Right, representative fluorescent microscopic images of the myotubes and quantified diameters of the myotubes (500 < n < 510).

(H) Effects of ectopic KLF15 expression on mTOR activity and myofiber cross-sectional area (CSA) in rat tibialis anterior. Left, representative immunoblots and quantified band densities (n = 5). Right, immunostaining for type IIB myosin heavy chain (MHC IIB, red in left photographs), type I myosin heavy chain (MHC I, red in right photographs), and type IV collagen (green) of transverse cryosections. CSA distribution of MHC IIB fibers (left) and MHC I fibers (right) are presented as frequency histograms (500 < n < 510).

(A–H) Error bars show SD. *$p < 0.05$, †$p < 0.05$ versus vehicle-treated rats. ‡$p < 0.05$ versus mock-transfected cells.

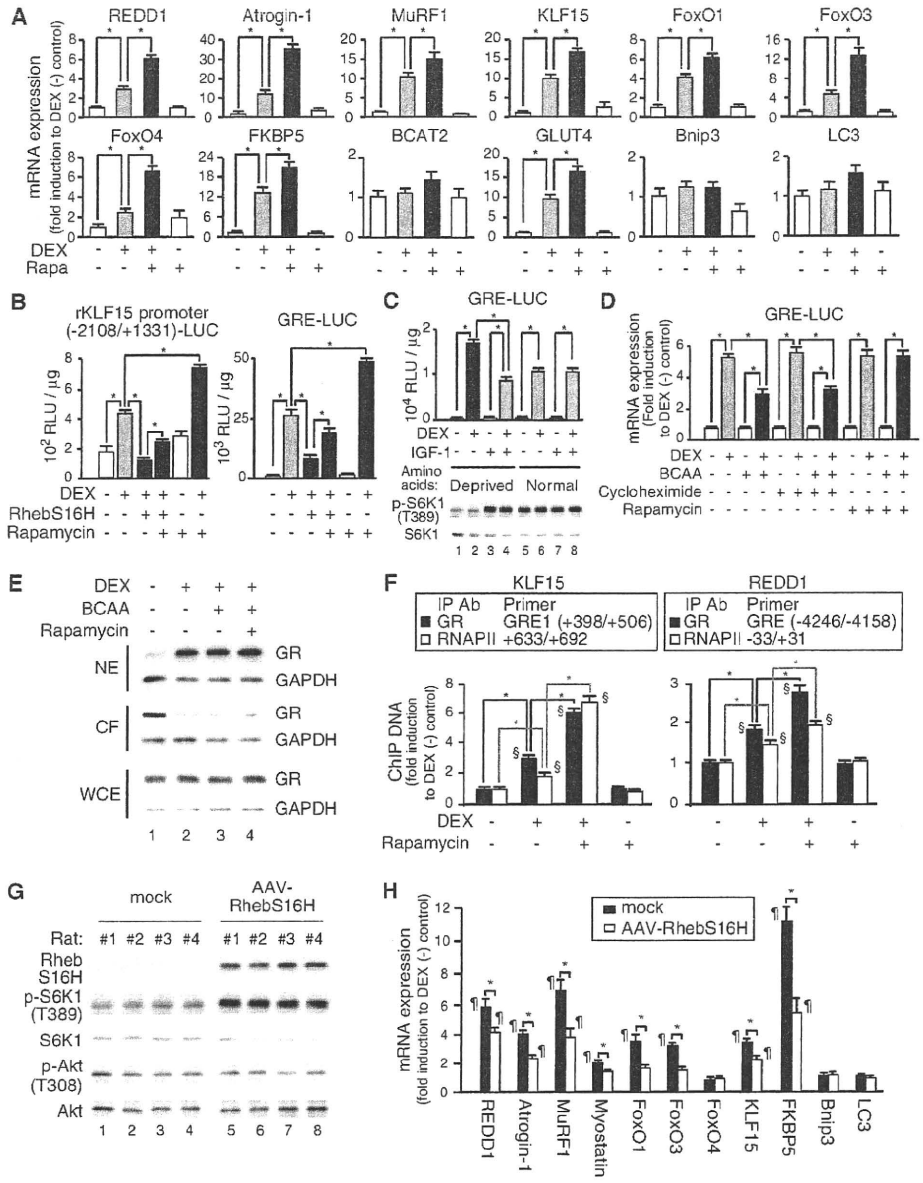

Figure 5. Negative Regulation of GR-Mediated Transcription by mTOR

(A) qRT-PCR analysis of L6 myotubes treated with DEX and rapamycin (Rapa) for 24 hr.

(B) Attenuation of GR-dependent reporter gene expression by mTOR. L6 myoblasts were transfected with rKLF15 promoter-LUC or GRE-LUC, with or without the expression plasmid for a constitutive active Rheb (RhebS16H), and treated with DEX and rapamycin for 18 hr.

(C) Effects of IGF-1 on mTOR activity and GR-dependent reporter gene expression. L6 myoblasts were transfected with GRE-LUC and cultured in amino acid-deprived DMEM (lanes 1–4) or normal DMEM (lanes 5–8) in the presence or absence of IGF-1 and/or DEX for 9 hr. Top, luciferase activities. Bottom, representative immunoblots.

(D) Effects of DEX, BCAA, cycloheximide, and rapamycin on GR-dependent reporter gene expression. L6 myoblasts were transfected with GRE-LUC and cultured in amino acid-deprived DMEM in the presence or absence of 10 mM BCAA cocktail, cycloheximide, rapamycin, and DEX for 6 hr.

(E) Effects of DEX, BCAA, and rapamycin on protein levels and subcellular localization of GR. L6 myotubes were cultured in amino acid-deprived DMEM in the presence or absence of DEX, 10 mM BCAA cocktail, and rapamycin for 30 min. Representative immunoblots of the nuclear extracts (NE), cytoplasmic fractions (CF), and whole-cell extracts (WCE) are shown (n = 3).

(F) Effects of rapamycin on DEX-dependent recruitment of GR onto target gene promoters. L6 myotubes were treated with 1 µM DEX and rapamycin for 2 hr (for KLF15) or 20 min (for REDD1) and processed for ChIP assays.

(G and H) Effects of ectopic expression of RhebS16H on mTOR activity and DEX-mediated mRNA expression. AAV-RhebS16H was infected to rat tibialis anterior for 7 days. (G) Representative immunoblots (n = 7). (H) qRT-PCR analysis of the muscles from the rats 6 hr after intraperitoneal injection with DEX.

(A–D, F, and H) Error bars show SD (n = 5). *$p < 0.05$, §$p < 0.05$ versus ChIP with normal IgG, ¶$p < 0.05$ versus vehicle-treated rats.

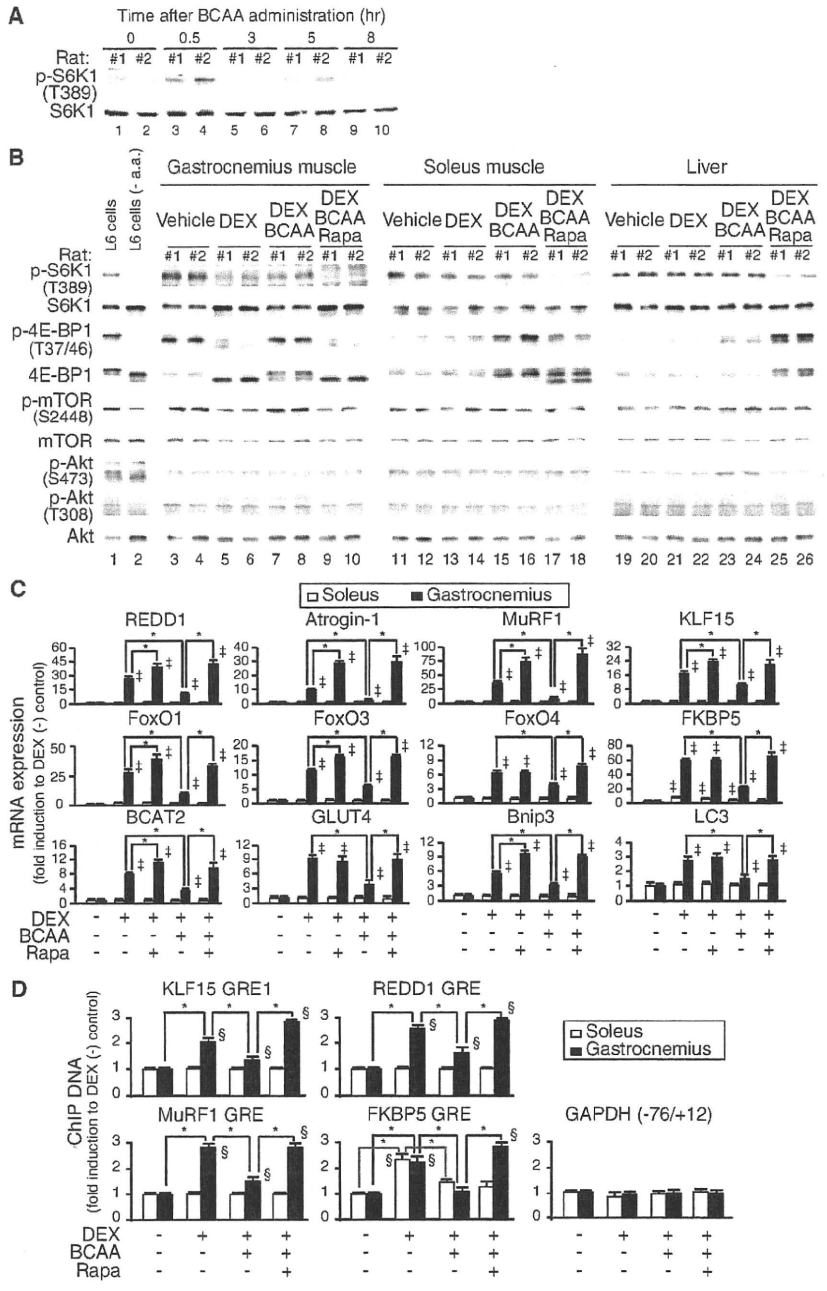

Figure 6. In Vivo Activation of mTOR and Attenuation of GR-Mediated Transcription after Programmed Administration of BCAA

(A) Time course of mTOR activity in rat gastrocnemius after BCAA administration. Representative immunoblots are shown (n = 5).

(B–D) Effects of DEX, BCAA, and rapamycin on mTOR activity; mRNA expression of atrophy-related genes; and GR recruitment onto the target gene promoters. Rats were treated with DEX, BCAA cocktail, and rapamycin for 5 days as described in the Supplemental Information. (B) Representative immunoblots (n = 17). L6 myotubes cultured in normal DMEM and in amino acid-deprived DMEM (−a.a.) for 1 hr were served as controls. (C) mRNA expression of atrophy-related genes. (D) Recruitment of GR onto its target genes. ChIP was performed using anti-GR antibody.

(C and D) Error bars show SD (n = 17). *$p < 0.05$, ‡$p < 0.05$ versus vehicle-treated rats, §$p < 0.05$ versus ChIP with normal IgG.

In skeletal muscle, this nutrition sensor-driven inhibition of GR function may be one of the mechanisms by which nutrients modulate the internal cellular milieu. Intriguingly, GR-mediated transcription was not repressed by insulin/IGF-1 under normal culture conditions, but did so when amino acids were deprived from the culture media (Figure 5C). This indicates that mTOR may be constitutively activated to a certain extent by nutrients and growth factors to protect cells from GR-driven catabolism in skeletal muscle. Under fasting conditions, however, blood concentrations of insulin/IGF-1 are low, and glucocorticoids may be allowed to efficiently drive the catabolic atrophy program for nutrient supply. Thus, our hypothesis may provide an insight into how muscle cells critically determine their volume after sensing endocrine hormones and the nutritional conditions for homeostatic regulation. In this context, GR-mTOR crosstalk might be a key for creating an interdisciplinary research area that bridges nutrition and medicine.

Therefore, the mTOR-mediated inhibition of GR in skeletal muscle is likely to be due not to the modulation of its chaperone activity but to its intervention in the access of GR to target DNA. It is becoming apparent that mTOR is intimately involved with the transcriptional apparatus in concert with a variety of transcription factors and cofactors (Cunningham et al., 2007). Since mTOR is reported to dock in the nucleus in association with, for example, PML (Bernardi et al., 2006), it would be of particular interest to identify such a factor that tethers GR and mTOR in the nucleus.

The biochemical rationale for the usage of BCAA as a therapeutic tool in glucocorticoid-induced muscle atrophy is that BCAA increases the association between Rheb and mTOR and, at least in part, mimics the effect of Rheb overexpression (Sancak et al., 2010). In our model, BCAA administration repressed mRNA expression of almost all GR-regulated genes (Figure 6C). ChIP analysis strongly supported the notion that BCAA administration inhibited GR recruitment onto the promoters of its target genes (Figure 6D). Moreover, these effects of BCAA were efficiently counteracted by rapamycin.

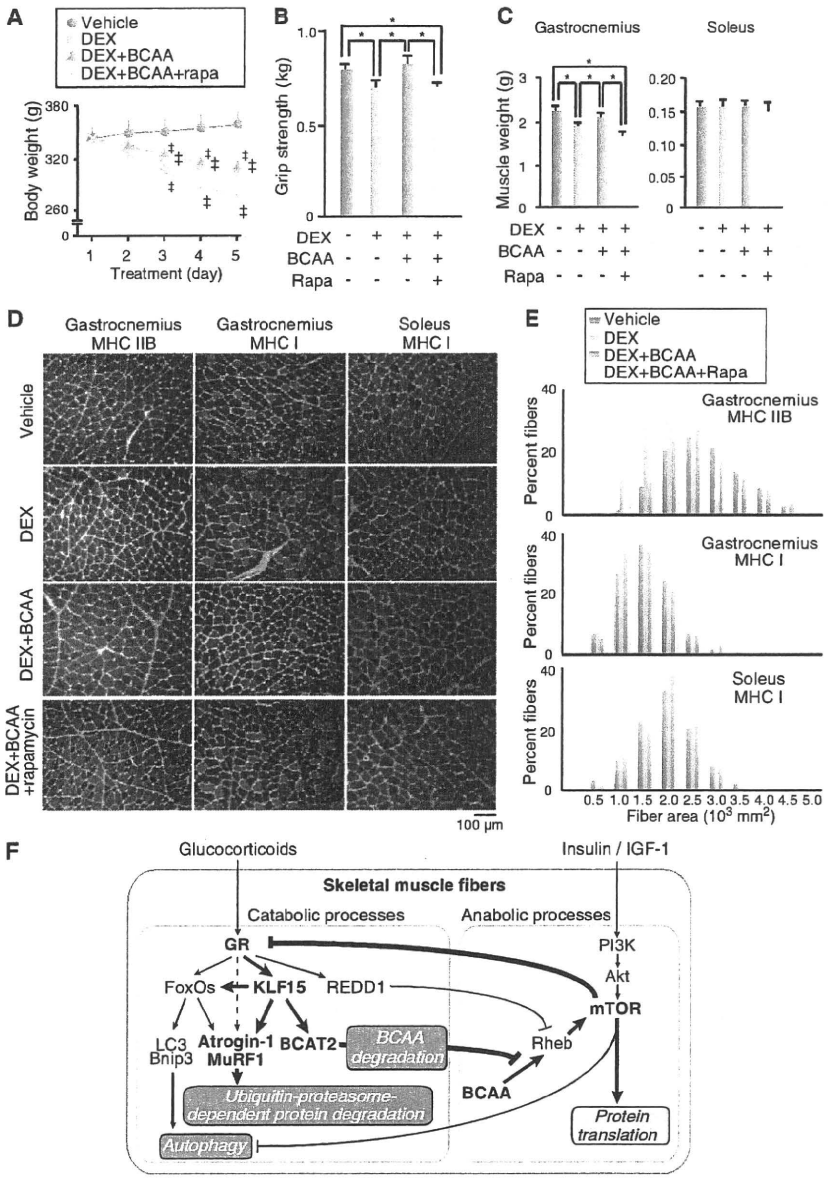

Figure 7. Restoration of Muscle Fiber Mass and Strength by mTOR Activation in DEX-Induced Skeletal Muscle Atrophy Model

(A–E) Effects of DEX, BCAA, and rapamycin on body weight (A), grip strength of forearms (B), muscle weight (C), muscle pathology (D), and CSA of skeletal muscle fiber (E). Rats were treated with DEX, BCAA, and rapamycin for 5 days as described in the Supplemental Information. (A) Time course of body weight ($n = 15$). (B) Grip strength of forearms at 5 hr after DEX injection on the day 5 ($47 < n < 51$). (C) Weight of gastrocnemius and soleus at 6 hr after DEX injection on the day 5 ($n = 15$). (D) Immunostaining for MHC IIB (red in left photographs), MHC I (red in middle and right photographs), and type IV collagen (green) of transverse cryosections. (E) CSA distribution of MHC IIB fibers (gastrocnemius) and MHC I fibers (gastrocnemius and soleus) presented as frequency histograms ($500 < n < 510$).

(F) Schematic model of mutual crosstalk between catabolic processes and anabolic processes in skeletal muscle.

(A–C) Error bars show SD (A and C) or SEM (B). $^{*}p < 0.05$, $^{‡}p < 0.05$ versus vehicle-treated rats.

proximal part of the insulin signaling pathway (Um et al., 2006). Moreover, in obese humans, BCAA in association with a high-fat diet is linked to the elevation of insulin resistance (Newgard et al., 2009). On the other hand, it is suggested that an increase in type II fibers in obese mice may reduce fat mass and improve metabolic parameters (Izumiya et al., 2008). Therefore, it is necessary, for the validation of BCAA therapy, to evaluate the influence of long-term BCAA administration on various metabolic parameters.

In conclusion, we revealed that GR and mTOR act as catabolic and anabolic liaisons for skeletal muscle metabolism, respectively, and these molecules interact with each other at multiple levels. This issue would be of particular importance to understand the molecular mechanism underlying the regulation of the volume and metabolism of muscle and for the development of treatments for glucocorticoid-induced and wasting disorder-related skeletal muscle atrophy.

Therefore, we are convinced that the therapeutic effects of BCAA could, at least in part, be ascribed to GR inhibition by the BCAA-mediated activation of mTOR. BCAA administration also resulted in the decreased mRNA expression of autophagy-related genes (Figure 6C), indicating that this therapeutic regimen repressed the vicious circuit connecting the initial induction of GR-triggered gene expression to degradation and atrophy. Of course, we cannot rule out other mechanisms for the effects of BCAA, including the non-GR-mediated repression of atrophy and/or autophagy, and further studies are clearly needed to clarify this issue.

There are conflicting results concerning the biological effects of BCAA, e.g., the overactivation of amino acid-dependent mTOR-mediated signaling can lead to the inhibition of the

EXPERIMENTAL PROCEDURES

Rats

All animal experiments were approved by the institutional committee and conducted according to the institutional ethical guidelines for animal experiments. Rapamycin, RU486, the BCAA cocktail, and DEX administration were performed as described in the Supplemental Information. Excised tissues were snap frozen in isopentane cooled by liquid nitrogen, and crushed using Cryo-Press (Microtec, Funabashi, Japan) prefrozen in liquid nitrogen, or processed to serial 10 μm transverse cryostat sections.

Cell Culture

L6 rat myoblasts, C2C12 mouse myoblasts, and COS-7 cells were obtained from American Type Culture Collection (Manassas, VA) and maintained in DMEM supplemented with 10% fetal bovine serum (Invitrogen, Carlsbad, CA). Culture conditions for myotube formation, drug treatment, and amino acids deprivation are described in the Supplemental Information.

In Silico Promoter Analysis

Putative FoxO1- and FoxO3-binding sequences, as well as putative GREs which are conserved between rat and human genomes, were searched for in the genomic regions (−5000 to +2000) of KLF15, REDD1, atrogin-1, and MuRF1 using rVISTA 2.0 as described in the Supplemental Information. KLF15-binding sequences (see the Supplemental Information) were searched for in the promoters of rat atrogin-1 (−4141 to +1191) and MuRF1 (−3223 to +1547) genes.

Chromatin Immunoprecipitation Assay

Cells or crushed tissues were treated with 1% formaldehyde in PBS for 10 min at 37°C, incubated in 125 mM glycine for 5 min, resuspended in buffer S (50 mM Tris [pH 8.0], 1% SDS, 10 mM EDTA) supplemented with 1 mM DTT, 100 nM MG132, and protease and phosphatase inhibitor cocktail (Nacalai Tesque, Kyoto, Japan), and incubated at 10°C for 10 min. Samples were sheared to an average size of 500 bp by sonication. Lysates corresponding to 2×10^6 cells or 200 mg of crushed tissues were diluted 10-fold in buffer D (0.01% SDS, 1.1% Triton X-100, 1.2 mM EDTA, 16.7 mM Tris [pH 8.1], 167 mM NaCl) supplemented with 100 nM MG132, and protease and phosphatase inhibitor cocktail, and incubated with 5 μg of antibodies listed in the Supplemental Information at 4°C for 18 hr. Protein A or G agarose/salmon sperm DNA (Millipore, Billerica, MA) was added and further incubated at 4°C for 1 hr. Precipitated DNA were quantified as described in the Supplemental Information.

Indirect Immunofluorescent Staining and Fluorescence Imaging

Muscle cryosections were treated with 0.1% Triton X-100, blocked with 5% goat serum/1% BSA in PBS, and incubated with antibodies listed in the Supplemental Information. After washing with PBS, specimens were incubated with secondary antibodies labeled with Alexa Fluor 488 or Alexa Fluor 568 (Invitrogen, 1:1000) and analyzed as described in the Supplemental Information. For imaging cultured myotubes, GFP was expressed in myotubes by infecting 10 multiplicity of infection of Ax1CAgfp (RIKEN DNA Bank, Tsukuba, Japan).

Statistical Analysis

Data were analyzed with Student's t test for unpaired data. P values below 0.05 were considered statistically significant. Graphs represent means ± SD or means ± SEM as specified in each figure legend.

SUPPLEMENTAL INFORMATION

Supplemental Information include one figure, Supplemental Experimental Procedures, and Supplemental References and can be found with this article at doi:10.1016/j.cmet.2011.01.001.

ACKNOWLEDGMENTS

This work was supported by Grants-in-Aid for Scientific Research, (to H.T., N.S., and N.Y.) and by grants from the Ministry of Health, Labour, and Welfare and from Japan Science and Technology Agency, Japan (to H.T.). Y.T., S.N., and K.T. are employees of Ajinomoto Pharmaceutical Company.

Received: June 17, 2010
Revised: October 14, 2010
Accepted: December 30, 2010
Published: February 1, 2011

REFERENCES

Aftring, R.P., Miller, W.J., and Buse, M.G. (1988). Effects of diabetes and starvation on skeletal muscle branched-chain alpha-keto acid dehydrogenase activity. Am. J. Physiol. *254*, E292–E300.

Beesley, A.H., Firth, M.J., Ford, J., Weller, R.E., Freitas, J.R., Perera, K.U., and Kees, U.R. (2009). Glucocorticoid resistance in T-lineage acute lymphoblastic leukaemia is associated with a proliferative metabolism. Br. J. Cancer *100*, 1926–1936.

Bentzinger, C.F., Romanino, K., Cloetta, D., Lin, S., Mascarenhas, J.B., Oliveri, F., Xia, J., Casanova, E., Costa, C.F., Brink, M., et al. (2008). Skeletal muscle-specific ablation of raptor, but not of rictor, causes metabolic changes and results in muscle dystrophy. Cell Metab. *8*, 411–424.

Bernardi, R., Guernah, I., Jin, D., Grisendi, S., Alimonti, A., Teruya-Feldstein, J., Cordon-Cardo, C., Simon, M.C., Rafii, S., and Pandolfi, P.P. (2006). PML inhibits HIF-1alpha translation and neoangiogenesis through repression of mTOR. Nature *442*, 779–785.

Csibi, A., Cornille, K., Leibovitch, M.P., Poupon, A., Tintignac, L.A., Sanchez, A.M., and Leibovitch, S.A. (2010). The translation regulatory subunit eIF3f controls the kinase-dependent mTOR signaling required for muscle differentiation and hypertrophy in mouse. PLoS ONE *5*, e8994. 10.1371/journal.pone.0008994.

Cunningham, J.T., Rodgers, J.T., Arlow, D.H., Vazquez, F., Mootha, V.K., and Puigserver, P. (2007). mTOR controls mitochondrial oxidative function through a YY1-PGC-1alpha transcriptional complex. Nature *450*, 736–740.

DeYoung, M.P., Horak, P., Sofer, A., Sgroi, D., and Ellisen, L.W. (2008). Hypoxia regulates TSC1/2-mTOR signaling and tumor suppression through REDD1-mediated 14-3-3 shuttling. Genes Dev. *22*, 239–251.

Evans, R.M. (2005). The nuclear receptor superfamily: a rosetta stone for physiology. Mol. Endocrinol. *19*, 1429–1438.

Fisch, S., Gray, S., Heymans, S., Haldar, S.M., Wang, B., Pfister, O., Cui, L., Kumar, A., Lin, Z., Sen-Banerjee, S., et al. (2007). Kruppel-like factor 15 is a regulator of cardiomyocyte hypertrophy. Proc. Natl. Acad. Sci. USA *104*, 7074–7079.

Gilson, H., Schakman, O., Combaret, L., Lause, P., Grobet, L., Attaix, D., Ketelslegers, J.M., and Thissen, J.P. (2007). Myostatin gene deletion prevents glucocorticoid-induced muscle atrophy. Endocrinology *148*, 452–460.

Glass, D.J. (2003). Signalling pathways that mediate skeletal muscle hypertrophy and atrophy. Nat. Cell Biol. *5*, 87–90.

Gray, S., Wang, B., Orihuela, Y., Hong, E.G., Fisch, S., Haldar, S., Cline, G.W., Kim, J.K., Peroni, O.D., Kahn, B.B., and Jain, M.K. (2007). Regulation of gluconeogenesis by Krüppel-like factor 15. Cell Metab. *5*, 305–312.

Gu, L., Gao, J., Li, Q., Zhu, Y.P., Jia, C.S., Fu, R.Y., Chen, Y., Liao, Q.K., and Ma, Z. (2008). Rapamycin reverses NPM-ALK-induced glucocorticoid resistance in lymphoid tumor cells by inhibiting mTOR signaling pathway, enhancing G1 cell cycle arrest and apoptosis. Leukemia *22*, 2091–2096.

Hoffman, E.P., and Nader, G.A. (2004). Balancing muscle hypertrophy and atrophy. Nat. Med. *10*, 584–585.

Hu, Z., Wang, H., Lee, I.H., Du, J., and Mitch, W.E. (2009). Endogenous glucocorticoids and impaired insulin signaling are both required to stimulate muscle wasting under pathophysiological conditions in mice. J. Clin. Invest. *119*, 3059–3069.

Hundal, H.S., Babij, P., Taylor, P.M., Watt, P.W., and Rennie, M.J. (1991). Effects of corticosteroid on the transport and metabolism of glutamine in rat skeletal muscle. Biochim. Biophys. Acta *1092*, 376–383.

Izumiya, Y., Hopkins, T., Morris, C., Sato, K., Zeng, L., Viereck, J., Hamilton, J.A., Ouchi, N., LeBrasseur, N.K., and Walsh, K. (2008). Fast/Glycolytic muscle fiber growth reduces fat mass and improves metabolic parameters in obese mice. Cell Metab. *7*, 159–172.

Ma, K., Mallidis, C., Artaza, J., Taylor, W., Gonzalez-Cadavid, N., and Bhasin, S. (2001). Characterization of 5′-regulatory region of human myostatin gene: regulation by dexamethasone in vitro. Am. J. Physiol. Endocrinol. Metab. *281*, E1128–E1136.

Mammucari, C., Milan, G., Romanello, V., Masiero, E., Rudolf, R., Del Piccolo, P., Burden, S.J., Di Lisi, R., Sandri, C., Zhao, J., et al. (2007). FoxO3 controls autophagy in skeletal muscle in vivo. Cell Metab. *6*, 458–471.

Matthews, S.E. (1999). Proteins and amino acids. In Modern Nutrition and Health and Diseases, 9th ed., M.E. Shils, J.A. Olson, M. Shike, and A.C. Ross, eds. (Baltimore: Williams & Wilkins), pp. 11–48.

Meijsing, S.H., Pufall, M.A., So, A.Y., Bates, D.L., Chen, L., and Yamamoto, K.R. (2009). DNA binding site sequence directs glucocorticoid receptor structure and activity. Science *324*, 407–410.

Menconi, M., Fareed, M., O'Neal, P., Poylin, V., Wei, W., and Hasselgren, P.O. (2007). Role of glucocorticoids in the molecular regulation of muscle wasting. Crit. Care Med. *35*, S602–S608.

Mizushima, N., Levine, B., Cuervo, A.M., and Klionsky, D.J. (2008). Autophagy fights disease through cellular self-digestion. Nature *451*, 1069–1075.

Moresi, V., Williams, A.H., Meadows, E., Flynn, J.M., Potthoff, M.J., McAnally, J., Shelton, J.M., Backs, J., Klein, W.H., Richardson, J.A., et al. (2010). Myogenin and class II HDACs control neurogenic muscle atrophy by inducing E3 ubiquitin ligases. Cell *143*, 35–45.

Munck, A., Guyre, P.M., and Holbrook, N.J. (1984). Physiological functions of glucocorticoids in stress and their relation to pharmacological actions. Endocr. Rev. *5*, 25–44.

Newgard, C.B., An, J., Bain, J.R., Muehlbauer, M.J., Stevens, R.D., Lien, L.F., Haqq, A.M., Shah, S.H., Arlotto, M., Slentz, C.A., et al. (2009). A branched-chain amino acid-related metabolic signature that differentiates obese and lean humans and contributes to insulin resistance. Cell Metab. *9*, 311–326.

Ning, Y.M., and Sanchez, E.R. (1993). Potentiation of glucocorticoid receptor-mediated gene expression by the immunophilin ligands FK506 and rapamycin. J. Biol. Chem. *268*, 6073–6076.

Risson, V., Mazelin, L., Roceri, M., Sanchez, H., Moncollin, V., Corneloup, C., Richard-Bulteau, H., Vignaud, A., Baas, D., Defour, A., et al. (2009). Muscle inactivation of mTOR causes metabolic and dystrophin defects leading to severe myopathy. J. Cell Biol. *187*, 859–874.

Sancak, Y., Bar-Peled, L., Zoncu, R., Markhard, A.L., Nada, S., and Sabatini, D.M. (2010). Ragulator-Rag complex targets mTORC1 to the lysosomal surface and is necessary for its activation by amino acids. Cell *141*, 290–303.

Sandri, M. (2008). Signaling in muscle atrophy and hypertrophy. Physiology (Bethesda) *23*, 160–170.

Sandri, M., Sandri, C., Gilbert, A., Skurk, C., Calabria, E., Picard, A., Walsh, K., Schiaffino, S., Lecker, S.H., and Goldberg, A.L. (2004). Foxo transcription factors induce the atrophy-related ubiquitin ligase atrogin-1 and cause skeletal muscle atrophy. Cell *117*, 399–412.

Schakman, O., Gilson, H., and Thissen, J.P. (2008). Mechanisms of glucocorticoid-induced myopathy. J. Endocrinol. *197*, 1–10.

Sengupta, S., Peterson, T.R., and Sabatini, D.M. (2010). Regulation of the mTOR complex 1 pathway by nutrients, growth factors, and stress. Mol. Cell *40*, 310–322.

She, P., Reid, T.M., Bronson, S.K., Vary, T.C., Hajnal, A., Lynch, C.J., and Hutson, S.M. (2007). Disruption of BCATm in mice leads to increased energy expenditure associated with the activation of a futile protein turnover cycle. Cell Metab. *6*, 181–194.

Stitt, T.N., Drujan, D., Clarke, B.A., Panaro, F., Timofeyva, Y., Kline, W.O., Gonzalez, M., Yancopoulos, G.D., and Glass, D.J. (2004). The IGF-1/PI3K/Akt pathway prevents expression of muscle atrophy-induced ubiquitin ligases by inhibiting FOXO transcription factors. Mol. Cell *14*, 395–403.

Suzuki, N., Motohashi, N., Uezumi, A., Fukada, S., Yoshimura, T., Itoyama, Y., Aoki, M., Miyagoe-Suzuki, Y., and Takeda, S. (2007). NO production results in suspension-induced muscle atrophy through dislocation of neuronal NOS. J. Clin. Invest. *117*, 2468–2476.

Um, S.H., D'Alessio, D., and Thomas, G. (2006). Nutrient overload, insulin resistance, and ribosomal protein S6 kinase 1, S6K1. Cell Metab. *3*, 393–402.

Waddell, D.S., Baehr, L.M., van den Brandt, J., Johnsen, S.A., Reichardt, H.M., Furlow, J.D., and Bodine, S.C. (2008). The glucocorticoid receptor and FOXO1 synergistically activate the skeletal muscle atrophy-associated MuRF1 gene. Am. J. Physiol. Endocrinol. Metab. *295*, E785–E797.

Wagenmakers, A.J. (1998). Protein and amino acid metabolism in human muscle. Adv. Exp. Med. Biol. *441*, 307–319.

Wang, H., Kubica, N., Ellisen, L.W., Jefferson, L.S., and Kimball, S.R. (2006). Dexamethasone represses signaling through the mammalian target of rapamycin in muscle cells by enhancing expression of REDD1. J. Biol. Chem. *281*, 39128–39134.

Yan, H., Frost, P., Shi, Y., Hoang, B., Sharma, S., Fisher, M., Gera, J., and Lichtenstein, A. (2006a). Mechanism by which mammalian target of rapamycin inhibitors sensitize multiple myeloma cells to dexamethasone-induced apoptosis. Cancer Res. *66*, 2305–2313.

Yoshikawa, N., Nagasaki, M., Sano, M., Tokudome, S., Ueno, K., Shimizu, N., Imoto, S., Miyano, S., Suematsu, M., Fukuda, K., et al. (2009). Ligand-based gene expression profiling reveals novel roles of glucocorticoid receptor in cardiac metabolism. Am. J. Physiol. Endocrinol. Metab. *296*, E1363–E1373.

Yu, L., McPhee, C.K., Zheng, L., Mardones, G.A., Rong, Y., Peng, J., Mi, N., Zhao, Y., Liu, Z., Wan, F., et al. (2010). Termination of autophagy and reformation of lysosomes regulated by mTOR. Nature *465*, 942–946.

Zhao, J., Brault, J.J., Schild, A., Cao, P., Sandri, M., Schiaffino, S., Lecker, S.H., and Goldberg, A.L. (2007). FoxO3 coordinately activates protein degradation by the autophagic/lysosomal and proteasomal pathways in atrophying muscle cells. Cell Metab. *6*, 472–483.